이학박사 학위논문

First-principles study on structural and electronic properties of silicene on $\sqrt{3} \times \sqrt{3}$ Si (111) - Ag (Au) monolayer

$\sqrt{3} \times \sqrt{3}$ Si (111) - Ag (Au) 단일 층 위에 놓인 실리신의 구조 및 전자적 성질에 관한 제일원리연구

2013년 8월

서울대학교 대학원

물리천문학부

최 근 수

First-principles study on structural and electronic properties of silicene on $\sqrt{3} \times \sqrt{3}$ Si (111) - Ag (Au) monolayer

$\sqrt{3} \times \sqrt{3}$ Si (111) - Ag (Au) 단일 층 위에 놓인 실리신의 구조 및 전자적 성질에 관한 제일원리연구

지도교수 임지순

이 논문을 이학박사 학위논문으로 제출함.

2013년 4월

서울대학교 대학원

물리천문학부

최 근 수

최근수의 이학박사 학위논문을 인준함.

2013년 6월

위 원 장 이 규 철 (인)

부위원장 임 지 순 (인)

위 원 강 병 남 (인)

위 원 민 홍 기 (인)

위 원 김 한 철 (인)

First-principles study on structural and electronic properties of silicene on $\sqrt{3} \times \sqrt{3}$ Si (111) - Ag (Au) monolayer

Keunsu Choi

Supervised by

Professor **Jisoon Ihm**

A Dissertation

Submitted to the Faculty of

Seoul National University

in Partial Fulfillment of

the Requirements for the Degree of

Doctor of Philosophy

August 2013

Department of Physics and Astronomy

Graduate School

Seoul National University

Abstract

Graphene, two-dimensional honeycomb lattice with C atoms, has attracted much attentions since it was synthesized in 2004 because of its peculiar sructural and electronic properties. Since Si atom also has same valence electrons with C atom, theoretical studies calculated the properties of two-dimensional honeycomb lattice with Si atoms and recent experiment has succeeded in synthesis of silicene on Ag (111) surface. Many researches have investigated in silicene that various superlattice structures on Ag (111) surface and the other metal substrates are found. Though silicene is expected to be promising nanoelectronics with experimental success, insulating substrate for silicene is still not reported yet. Furthermore, recent studies insist that the linear dispersion band measured form angle-resolved photo emission spectroscopy (ARPES) in above experiment is not originated from Si p_z orbital, but from the hybridization between Si and Ag atoms.

In this thesis, we analyse stuructural and electronic properties of freestanding silicene, silicene on metal substrate usgin *abinito* calculation and suggest the structure with silicene-insulating substrate. First, we show that bandgap of freestanding silicene can be opened through various processes because of its peculiar structure, light-buckling hexagonal lattice: (1) changing buckling pattern can open bandgap

since it breaks sublattice inversion symmetry. (2) applying electric field perpendicular to silicene plane also can open bandgap. Si atoms located on different heights feel different potential and hence have asymmetry wavefunction. (3) hybridization between silicene and substrate also can open bandgap. Practically, all the three process play a part in opening bandgap.

Analysing the amount of electrons in each atoms when silicene is formed on Ag (111) surface shows that the electrons from Ag substrate to Si atoms are 0.15e on average. Therefore, we can predict that silicene band in total electronic band structure shift down compared with freestanding silicene band. Projection of electronic band structure to Si p_z orbital reveals that π band shift down 1.2 eV from Fermi level and the linear dispersion band in previous experiment, which extends from -0.3 eV to -3 eV, is not originated from silicene. Silicene π band also shifts down when silicene is put on Au (111) surface and hybridization between Si and Au is stronger than that between Si and Ag. We calculate energy barrier of Si atom on substrate, because it play an important role in diffusion. The results are that Ag and ZrB_2 have similar values while Au has much less value. We can suggest from above results the magnitude of energy barrier for substrate in usual usual deposition conditions.

Finally, We propose insulating substrate consists of insulator and metal thin film. Ag thin film is used to make deposited Si atoms to form silicene as Ag (111) surface does. Since metal thin film interacts with underneath insulating substrate, hybridization between silicene and metal atoms also can be weaken that Dirac-electron character of silicene is not destroyed. Among a couple of candidates, we choose and investigate the structural and electronic properties of $\sqrt{3} \times \sqrt{3}$ Si (111) - Ag (Au) monolayer. Silicene on both substrate has bangap with $\sim$ 120 meV originated from

the three processes as mentioned above and hence off-current state can be realized with silicene. In sequence, We analyse the first conduction band by projecting it on orbital basis in order to see the contribution of Si p_z orbital, which can act as conduction channel. The Si p_z orbital character is dominant between K and Γ point at 0.2 eV. On-current state can be realized around this energy level. We show the possibility of silicene on substrate as nanoelectronics in this study.

Keywords : density functional theory, graphene, silicene, nanoelectronics, insulating substrate, bandgap, scanning tunneling microscopy

Student Number : 2002-20419

Contents

List of Acronyms

DFT density functional theory

LDA local density approximation

PAW projected augmented wave

GGA generalized gradient approximation

PBE Perdew-Burke-Erenzerhof

PAO pseudo-atomic orbital

LCAO linear combination of atomic orbitals

LEED low energy electron diffraction

2D two-dimensional

STM scanning tunneling microscopy

COOP crystal-orbital overlap projection

LB low buckling

List of Figures

List of Tables

Chapter 1

Introduction

Since graphene is successfully synthesized in 2004, two-dimensional materials have had much attractions from theoretic and experimental aspects. Its peculiar electronic and mechanical properties make it possible to reveal many interesting phenomena like klein tunneling, quantum hall effect, etc [4, 5]. Moreover, it is also very fascinating in view of industrial application because of massless dirac electron, which shows extremely fast fermi velocity. As an allotrope of graphene, freestanding monolayers with Silicon and Germanium atoms are also studied by theoretical calculation using density functional theory (DFT) method [6, 7]. Electronic band structures of two monolayers also show Dirac cone at K point like graphene. Since freestanding silicene is stable in low buckled structure, bandgap can be easily obtained by changing of buckling pattern, applying electric field and interacting with substrate as discussed in chapter 2 [**?**]. Silicene is expected to be promising materials as nanoelectronics that can replace graphene, because it has advantages not only in presence of Dirac-like electron for on-current state but also in bandgap for

off-current state. However, Si atoms strongly tend to aggregate to form bulk and can not exist in the form of freestanding 2D layer. Therefore suitable substrate is requisite in order to synthesize silicene and utilize it as nanoelectronics. After the theoretical predictions, many experimental researchs focused on synthesis of silicene on substrate and have succeed in various substrate [8, 9, 10, 11, 12]. First reliable synthesis of silicene was achieved on Ag (111) surface [8] that deposited Si atoms form 3×3 silicene superlattice on 4×4 Ag (111) surface. Angle-resolved photon emission (ARPES) measurement showed linear dispersion band of which fermi velocity ($\sim 1.3\times10^6$ m/s) derived from slope of linear band is comparable with fermi velocity of graphene. Following experimental researches found that many kinds of silicene superlattice can exist on Ag (111) surface and silicene can be synthesized on the other metal substrate (Ir(111) and $ZrB_2(001)$) [13, 1].

First, we introduce the basic properties of freestanding silicene and show various badgap opening mechanisms. Since freestanding silicene is stable in low buckled low buckled structure, bandgap can be opened easily compared with graphene. Since Dirac-cone is protected by sublattice inversion symmtry, changing of buclking pattern can break inversion symmetry and open bandgp. Appying electric field also gives similar results that electric field induces potential difference between top and bottom Si atoms and open bandgap proportion to potential difference. In chapter 3, silicene on metallic substrate (Ag, Au and ZrB_2) will be investigated using *ab initio* calculations. Analysis in structural and electronic properties of silicene on metal substrate, on which already silicne is synthesized, and calculation of binding energy and energy barrier between Si atoms and substrate can give guideline in desiging insulating substrate for siliceen. In chapter 4, we investigate for the system that sil-

icene on $\sqrt{3} \times \sqrt{3}$ Si(111) - Ag (Au) monolayer. Since the metal layers are inhomogeneous, buckling pattern of silicene changes and it contributes to bandgap opening. Projection of wavefuntion obtained in plane-wave basis to orbital basis gives the information how much the orbital of specific atom contribute to band structure. We analyze the first conduction band and find that π band originated from Si p_z orbital is dominate at 0.2 eV. We can realize on-current state with silicene and hence shows possibility of silicene as nanoelectronics.

Chapter 2

Basic properties of silicene

Considering the number of valence electrons, Si and Ge atoms are also investigated the possibility in formation of 2-dimensional lattice like graphene. From the theoretical DFT calculations, freestanding silicene and germanene is predicted to be stable in light buckled 2-D hexagonal structure – single layer with Ge atom [6, 7]. Silicene has two Si atoms (top and bottom) in primitive unit cell like graphene with bond length 2.29Å, but two Si atoms have different heights with 0.44Åas shown in fig. 2.3 (a). It is due to the relatively long bond lengths, because weak bond strength makes it hard to form planar structure. Though freestanding silicene is stable in low-buclked structre, tight-binding description of graphene can be good starting point to describe silicene, since silicene also has 2D hoenycomb lattice.

2.1 Tight-binding model description of graphene

2.1.1 Electronic band calculation

In the tight binding (TB) model, it is assumed that the full Hamiltonian H of the system may be approximated by the Hamiltonian with the basis of atomic orbitals (ϕ_i) at lattice points. TB method is solving generalized eigenvalue problem by expanding wave function with ϕ

$$H\Psi = ES\Psi \tag{2.1}$$

If some orbitals in given system are separated from others, the electronic structure which is originated from the separated orbital is well described by tight-bindig (TB) model. Before derive the general formula. Let's start with the simple two dimensional system, graphene. Graphene, a carbon allotrope, is a two-dimensional hexagonal network of carbon atoms which is formed by making strong triangular σ-bonds of the sp^2 hybridized orbitals. The π-orbitals orthogonal to the hexagonal plane of graphene are responsible for its characteristic electronic properties around the Fermi level (E_F).

Among the valence orbitals of carbon, $2s$ and $2p$, p_z orbital is perfectly separated from other orbitals and the electronic structue around the Fermi level (E_F) is determined by p_z. The crystal structure of graphene is hexagonal with two basis atoms. We use only one p_z orbital per one atom. In order to describe crystal, we use the Bloch theorem and change the basis with crystal momentum k as follows [**?** **?**]:

$$\phi_{k,\alpha}(r) = \frac{1}{\sqrt{N}} \sum_n e^{ik\cdot T_n} \phi(r - x_i - T_n), \ (\alpha = A, B) \tag{2.2}$$

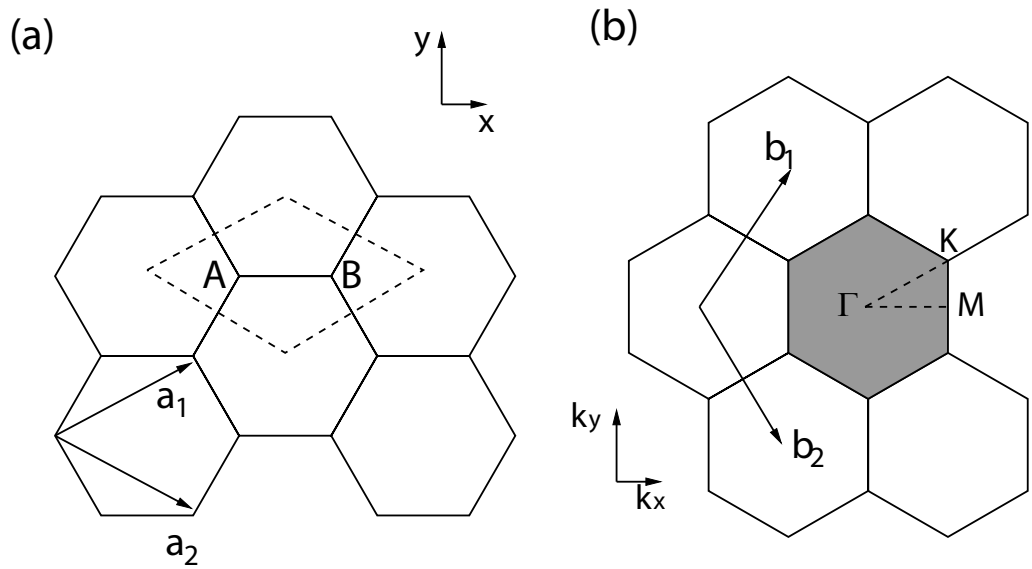

Figure 2.1: (a) The unit cell and (b) Brillouin zone of two-dimensional graphite are shown as the dotted rhombus and the shaded hexagon, respectively. a_i and b_i, $(i = 1, 2)$ are unit vectors and reciprocal lattice vectors, respectively.

where the summation is taken over the atomic site coordinate T_n for the A or B carbon atoms in a unit cell of graphite. N is the number of unitcells. The full Hamiltonian matrix is bolk diagonalized into 2×2 matrix with k, $H_{\alpha,\beta}(k)$. By considering nearest neighbor hopping only we obtain

$$H(k) = \begin{pmatrix} \epsilon_{2_p} & f(k) \\ f^*(k) & \epsilon_{2_p} \end{pmatrix}, \tag{2.3}$$

where ϵ_{2_p} is the orbital energy of the $2p$ level which is difined as $\langle p_z|H|p_z\rangle$, and $f(k)$ is

$$f(k) = \frac{1}{N}\sum_{n,n'} e^{ik\cdot(T_n - T_{n'})}\langle p_z(r - T_n - r_A)|H|p_z(r - T_{n'} - r_B)\rangle \quad (2.4)$$

$$= -t(1 + e^{-ik\cdot a_1} + e^{-ik\cdot a_2}) \quad (2.5)$$

t is the nearest neighbor hopping integral ($\approx 2.7eV$). By assuming $S = 1$, eigenvaluses of graphene are

$$E(k_x, k_y) = \epsilon_{2_p} \pm t\sqrt{1 + 4\cos\frac{\sqrt{3}k_x a}{2}\cos\frac{k_y a}{2} + 4\cos^2\frac{k_y a}{2}}. \quad (2.6)$$

Fig.(2.2) is the band structure of graphene along the symmetry point. As this figure and Eq.(2.6), π band (i.e. the band below E_F) and π^* are symmetric, because we assume that overlap matrix is unity.

General tight binding Hamiltonian can be written as follow:

$$H = -\sum_{\langle i,j\rangle} t_{i,j} c_i^\dagger c_j + \sum_i U_i. \quad (2.7)$$

where $t_{i,j}$ is the hopping integral between i and j sites, and U_i is on-site energy of i^{th} site. In many simple system, hopping integral is independent of i and j, however, our system is not the case. We use the following basis and wavefunction which satisfy the Bloch theorem.

$$\Psi_k(r) = \sum_i c_i(k)\tilde{\phi}_i(r, k) \quad (2.8)$$

$$\tilde{\phi}_i(k, r) = \frac{1}{\sqrt{N}}\sum_n e^{ik\cdot T_n}\phi(r - x_i - T_n) \quad (2.9)$$

where the k, T_n and N are Bloch wave vector, translation vector of n^{th} cell and the number of unitcells, respectively. $\phi(r - x_i - T_n)$ is the i^{th} atomic orbital in n^{th} cell

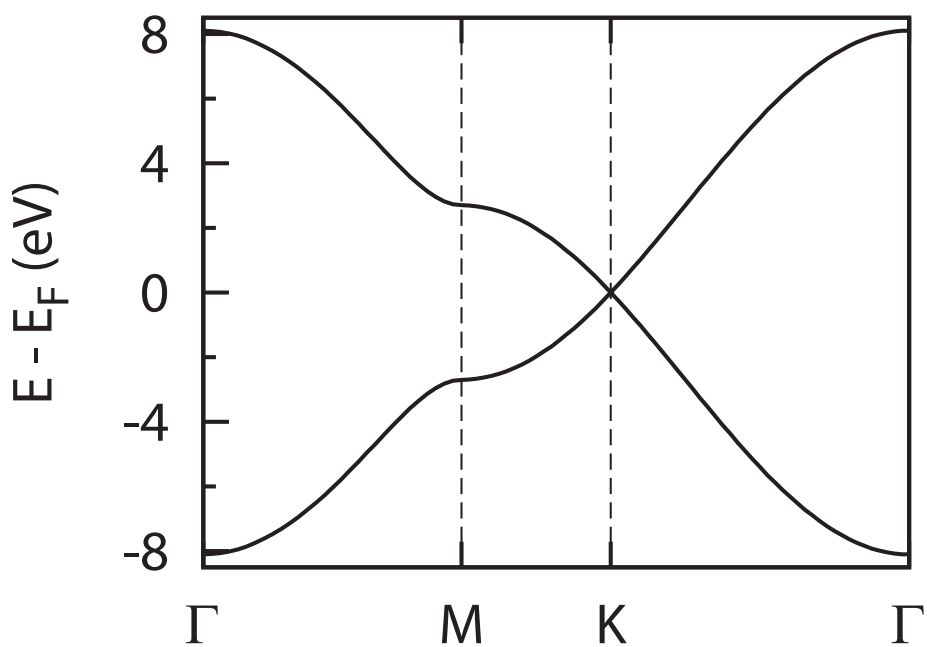

Figure 2.2: The p_z band structure of graphene. $t = 2.7$eV is used. Band structure is symmetric with respect to E_F since overlap matrix is ignored.

and $x_i + T_n$ is the position of i^{th} site in n^{th} unitcell. The summation is taken over the all atomic site in unicell. Both basis ($\tilde{\phi}$) and wavefunction (Ψ) satisfy Bloch theorem in this setting; $\psi(k, r+T) = e^{-ik\cdot T}\psi(k, r)$. The Hamiltonian matrix is

$$
\begin{aligned}
H_{ij} &= \langle\tilde{\phi}_i|H|\tilde{\phi}_j\rangle && (2.10)\\
&= \frac{1}{N}\sum_{n,m} e^{i\mathbf{k}\cdot(\mathbf{T}_n-\mathbf{T}_m)}\langle i,m|H|j,n\rangle && (2.11)\\
&= \begin{cases} -t_{i,j}\sum_n e^{i\mathbf{k}\cdot\mathbf{T}_n} & \text{if } |i,0\rangle \text{ and } |j,n\rangle \text{ are NN} \\ U_i & \text{if } i=j,\ n=m \\ 0 & \text{otherwise} \end{cases} && (2.12)
\end{aligned}
$$

If we ignore the nearest neighbor overlap integral $\langle\phi_i|\phi_j\rangle$, Eq.2.1 will be written in matrix form of $\sum_j H(k)_{ij}c_j = E(k)c_i(k)$. For large size of system this can be solved by numerical method.

Though sp2 and sp3 characters hybridize each other due to buckling, electronic band structure of silicene still has the Dirac-cone at K point. The D3 symmetry at K point in silicene is decreased one of D3h symmetry at K point in grapheme by the relation that $D_3h = D3 \times C_s$

Symmetry analysis also can prove that silicene has linear dispersion relation near K point with D3 and sublattice inversion symmetry [14].

The Fermi velocity of silicene can be obtained by calculating the slope of electronic band structure at Dirac-cone from the relation that

$$v_f = \frac{1}{m}\frac{\partial^2 E}{\partial k^2}.$$

The v_f obtained from fig. 2.3 (b) is order of $\sim 10^5$ m/s and is much less than that of graphene for weaker π bonds in silicene The fermi velocity can be corrected if many-body effect is considered.

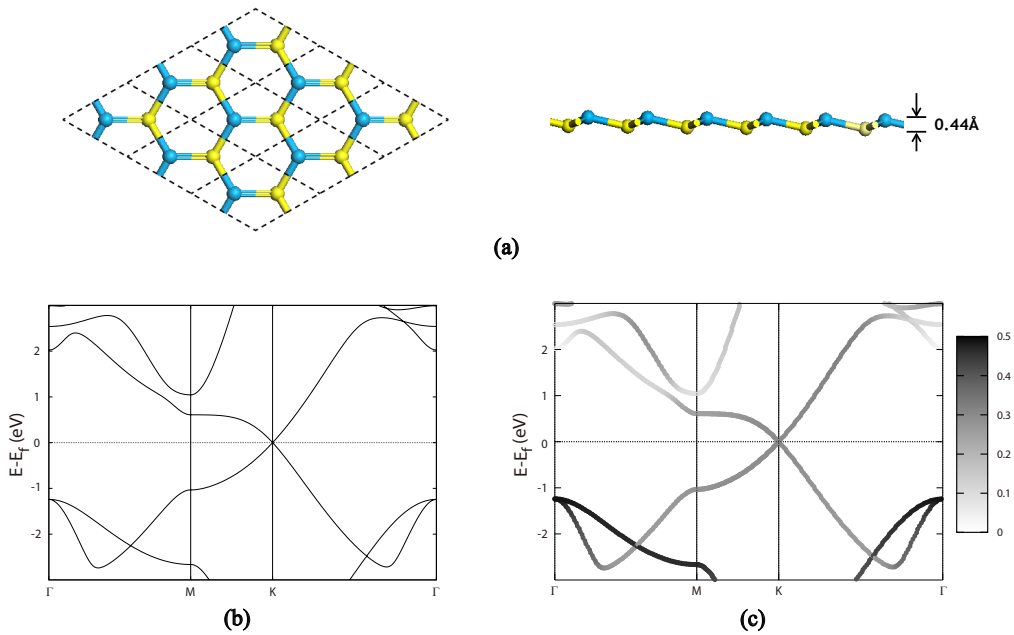

Figure 2.3: The structure of freestanding pristine silicene (FPS) is given with top (left) and side (right) views, which contains two Si atoms (top and bottom Si atoms are represented with cyan and yellow) in primitive unit cell (black dashed line) (a). The bond length and height difference between two Si atoms are 2.3Åand 4.4Å, respectively. Electronic band structure of FPS (b) and projections of corresponding wavefunctions to Si $3p_z$ orbital (c). π and π^* band originated from Si $3p_z$ orbitals constitute Dirac cone at Γ point.

2.2 bandgap opening

The bandgap of freestanding silicene can be opened through two mechanisms: 1) changing buckling pattern of silicene and 2) applying electric field perpendicular to silicene plane. When Si atoms are deposited on substrate to form silicene, surface structure of substrate are not perfectly commensurate with silicene and hence buckling patterns of FPS and deposited silicene are different. Since this change breaks sublattice inversion symmetry, bandgap of freestanding deformed silicene (FDS) can

be opened. The bandgap opening through this mechanism can be identified by deforming buckling pattern of $\sqrt{3} \times \sqrt{3}$ FPS that shifts up one bottom Si atom to top position. The structure of FDS is given in fig. 2.4 (a) that four Si atoms are in top position among six atoms. Figure 2.4 (b) and (c) show electronic band structures of $\sqrt{3} \times \sqrt{3}$ FPS and FDS, respectively. The Dirac-cone appears at Γ point in $\sqrt{3} \times \sqrt{3}$ FPS, because Dirac-cone at K point in primitive cell are folded into Γ point in $\sqrt{3} \times \sqrt{3}$ superlattice.

On the other hand, applying z-direction perpendicular to silicene plane can open bandgap for silicene because of its peculiar buckled layer structure [15]. Since Si atoms of silicene has different height, they have different on-site energy in view of tight-binding model. The difference of on-site energy leads bandgap,

$$\varepsilon = \sqrt{(\Delta/2)^2 + (v\mathbf{p})^2} \ , where \ \Delta = \varepsilon_A - \varepsilon_B$$

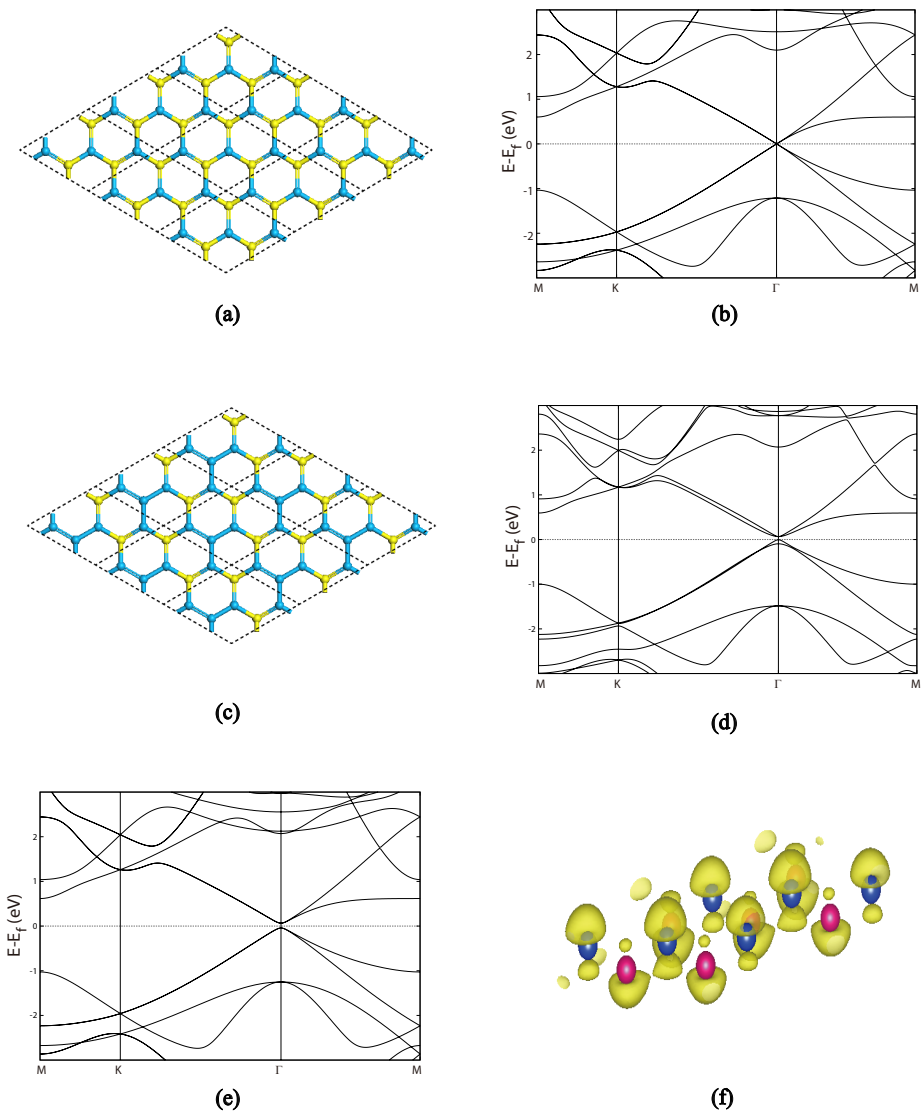

Figure 2.4: Bandgap opening in $\sqrt{3} \times \sqrt{3}$ silicene. The structures of FPS (a) and FDS (c) are same except the height of on Si atom (cyan and yellow represent top and bottom Si atoms like fig. 2.3 (a)). Comparing (b) and (d) around Γ point, which correspond to FPS and FDS, sublattice inversion symmetry breaking opens bandgap and break degeneracy in FDS. (e) Applying electric field (0.5eV/Å) perpendicular to FPS also open bandgap. Because top and bottom Si atoms feel different potential, it gives effective sublattice inversion symmetry breaking. (f) Asymmetry in charge densities of top (blue) and bottom (red) Si atoms under 0.5 eV/Åelectric field

Chapter 3

Computational methods

3.1 Introduction

Diverse properties of a condensed matter system can be understood by manifesting their electronic structures. Precise prediction of electronic structures has been always the most important goal of the condensed matter physics. In this respect, density functional theory (DFT) has been successful and now became the most wide spread and popular method to predict the electronic structures of a many-body system.

In principle, the properties of any (non-relativistic) time-independent quantum system can be determined by solving the Schrödinger equation,

$$\mathcal{H}\Psi(\mathbf{r}_1, \mathbf{r}_2, \ldots, \mathbf{r}_N) = E\Psi(\mathbf{r}_1, \mathbf{r}_2, \ldots, \mathbf{r}_N), \tag{3.1}$$

where, $\mathcal{H}$, Ψ and E are the Hamiltonian, many-body wavefunction and total energy of the system. Matter consists of electrons and nuclei interacting with each other via the Coulomb interaction, consequently the Hamiltonian for any such system is

given by,

$$\begin{aligned}\mathcal{H} = &-\sum_i \frac{\hbar^2}{2m_e}\nabla_i^2 - \sum_I \frac{\hbar^2}{2M_I}\nabla_I^2 \\ &+ \frac{1}{2}\sum_{I\neq J}\frac{Z_I Z_J e^2}{|\mathbf{R}_I - \mathbf{R}_J|} + \sum_{i,I}\frac{Z_I e^2}{|\mathbf{r}_i - \mathbf{R}_I|} + \frac{1}{2}\sum_{i\neq j}\frac{e^2}{|\mathbf{r}_i - \mathbf{r}_j|}\end{aligned} \tag{3.2}$$

The first two terms in (3.2) are the kinetic energy contributions from the nuclei and the electrons respectively, and the rest are Coulomb potential energy terms arising from the ion-ion repulsion, ion-electron attraction and the electron-electron repulsion respectively. However, the Schrödinger equation (3.1) is a many-body equation and difficult to solve directly. Density functional theory provides *a*d hoc. for this problem with great success. In this Chapter, The essence of density functional theory will be briefly reviewed. Readers who want more extensive and complete review can refer to the literatures [16, 17, 18], based on which this review is written.

3.2 Born-Oppenheimer Approximation

There is a large difference between the masses of electrons and nuclei. For the simplest nuclei, a single proton, the ratio of nuclei to electron masses is approximately 2000. Due to this, there is a large difference in the timescales of electronic and nuclear motion. This is the motivation for the Born-Oppen-heimer approximation. The difference in the masses allows the electrons to respond almost instantaneously to the motion of the nuclei. This allows the separation of the Hamiltonian into nuclear and electronic parts. Within the Born-Oppenheimer approximation the complexity of the full many-body Hamiltonian (3.2) reduces to that of an electronic Hamilto-

nian,

$$\mathcal{H} = -\sum_i \frac{\hbar^2}{2m_e}\nabla_i^2 + \sum_{i,I} \frac{Z_I e^2}{|\mathbf{r}_i - \mathbf{R}_I|} + \frac{1}{2}\sum_{i \neq j} \frac{e^2}{|\mathbf{r}_i - \mathbf{r}_j|} \tag{3.3}$$

Now, electronic structure calculations aim to solve the electronic Schrödinger equation (SE) as a function of the nuclear coordinates.

3.3 Density Functional Theory

density functional theory (DFT) is developed based on the fundamental tenet that the ground state properties of a given system can be determined by the ground state charge density [19, 20],

$$\rho(\mathbf{r}_1) = \int \Psi^*(\mathbf{r}_1, \mathbf{r}_2, \ldots, \mathbf{r}_n)\Psi(\mathbf{r}_1, \mathbf{r}_2, \ldots, \mathbf{r}_n) d\mathbf{r}_2 \cdots d\mathbf{r}_n, \tag{3.4}$$

where $\Psi(\mathbf{r}_1, \mathbf{r}_2, \ldots, \mathbf{r}_n)$ a many-body wavefunctions for the ground state. Any properties of a system of many interacting particles is considered to be a functional of the ground state density $\rho(\mathbf{r}_1)$, It is important to find the ground state density as well as a potential that generates the charge density. Solving the many-body problem in terms of charge density is advantageous over solving the problem based on wave function since a charge density is a scalar function of three spatial variable ($\vee r$) while a wavefunction of a function of $3N$ variables describing the positions of N electrons. The idea to treat the problem using a charge density goes back the early work of Thomas and Fermi [21]. They treated the energy as a functional of a charge density and energy is expected to be the summation of the kinetic energy of a uniform electron gas and the classical electrostatic interaction between the electrons and nuclei for an electron gas of a given energy. The idea of Thomas and Fermi

is later extended by adding the exchange energy of the electrons from the work of Dirac. However, it is turns out that the Thomas-Fermi theory generates poor results due to the inappropriate approximations in kinetic energy [21]. Later, Kohn, Hohenberg, and Sham [19, 20] described the kinetic energy in terms of wavefunctions instead of a charge density, as described below, and this treatment is turned out to be successful.

3.3.1 Hohenberg-Kohn theorem

According to the Hohenberg-Kohn theorem, the ground state properties of a many-electron system under an external potential v_{ext} can be uniquely determined by the electron density. The Hohenberg-Kohn theorem states:

Theorem 1. *The external potential v_{ext} is a unique functional of the electron density $n(\mathbf{r})$. Thus the Hamiltonian, and hence all ground state properties, are determined solely by the electron density.*

The many-body Hamiltonian $\mathcal{H}$ describes the ground state properties of a many-electron system by determining the ground state many-body wavefunction Ψ. This means that the Hohenberg-Kohn theorem guarantees that the kinetic energy and electron-electron interaction energy should also be functionals of the electron density $n(\mathbf{r})$. Therefore, one may define the energy functional

$$F[n(\mathbf{r})] = \langle \Psi | (T + V_{ee}) | \Psi \rangle. \tag{3.5}$$

Here T and V_{ee} are the kinetic energy operator and the electron-electron interaction operator, respectively. This functional F should be universal in the sense that it is independent of the external potential concerned. Although the explicit form of the

functional in terms of electron density is unknown, one may then define using this functional, for a given external potential $v_{\text{ext}}(\mathbf{r})$ as

$$E\left[n(\mathbf{r})\right] = \int d\mathbf{r} n(\mathbf{r}) v_{\text{ext}}(\mathbf{r}) + F\left[n(\mathbf{r})\right]. \tag{3.6}$$

Then, we may be able to write the energy (for a non-degenerate ground state) in terms of the ground state many-body wavefunction Ψ as

$$E\left[n(\mathbf{r})\right] = \langle \Psi \left| \mathcal{H} \right| \Psi \rangle \tag{3.7}$$

with the Hamiltonian given by

$$\mathcal{H} = F + V \tag{3.8}$$

where V is the operator corresponding to the external potential, and F is the electronic Hamiltonian

$$F = T + V_{ee}. \tag{3.9}$$

Proof. Suppose that there are two potentials $v_1(\mathbf{r})$ and $v_2(\mathbf{r})$, which differ each other by more than an additive constant, and these two potentials produce different ground state wavefunctions $\Psi_1(\mathbf{r})$ and $\Psi_2(\mathbf{r})$. Also suppose that these both potential give rise to the same ground state density, $n(\mathbf{r})$. The variational principle then dictates that

$$\begin{aligned} E_1 \leq \langle \Psi_2 \left| H_1 \right| \Psi_2 \rangle &= \langle \Psi_2 \left| H_2 \right| \Psi_2 \rangle + \langle \Psi_2 \left| H_1 - H_2 \right| \Psi_2 \rangle \\ &= E_2 + \int n(\mathbf{r}) \left[v_1(\mathbf{r}) - v_2(\mathbf{r}) \right] d\mathbf{r} \end{aligned} \tag{3.10}$$

Note that by interchanging the indices 1 and 2, one may obtain a similar expression, and by adding the two inequalities, we may draw a contradiction,

$$E_1 + E_2 \leq E_1 + E_2. \tag{3.11}$$

Hence the theorem 1 is proved. □

Theorem 2. *The ground state energy may be variationally obtained; the density that minimizes the total energy is the exact ground state density.*

Proof. In order to prove the theorem, let us first introduce the concept of "*N-representability*". One may say a density is N-representable whenever it can be obtained from an antisymmetric wavefunction $\psi(\mathbf{r}_1, \mathbf{r}_2, \ldots, \mathbf{r}_N)$, from which we may define the functional

$$F[n] = \min_{\psi \to n} \langle \psi | T + V_{\text{ee}} | \psi \rangle. \tag{3.12}$$

Here the minimum is taken over all the possible wave functions ψ which can generate the density n. Then if one introduces $\psi^n_{min}(\mathbf{r})$ for a wavefunction that minimizes (3.12) such that

$$F[n] = \langle \psi^n_{\text{min}} | T + V | \psi^n_{\text{min}} \rangle \tag{3.13}$$

then

$$\begin{aligned} \int V_{\text{ext}}(\mathbf{r}) n(\mathbf{r}) d\mathbf{r} + F[n] &= \langle \psi^n_{\text{min}} | V + T + V_{\text{ee}} | \psi^n_{\text{min}} \rangle \\ &\geq E_{\text{GS}} \end{aligned} \tag{3.14}$$

with equality at the minimum, which proves the second theorem. □

3.3.2 Kohn-Sham equation

Although the Hohenberg-Kohn theorem guarantees the existence of the ground state density determining the ground state properties of a many-body system, it does not provide a specific method to find the ground state density of the system. Walter

Kohn and Lu Jeu Sham [20] tackled this problem and provided a route toward a practical way to obtain the ground state density by constructing the Kohn-Sham equation. Suppose that the ground state energy is given as a functional of the charge density

$$E\left[\rho(\mathbf{r})\right] = T\left[\rho(\mathbf{r})\right] + \int \rho(\mathbf{r}) v(\mathbf{r})\, d\mathbf{r} + E_{ee}. \tag{3.15}$$

Here the first term $T\left[\rho(\mathbf{r})\right]$ is the kinetic energy functional, the second term is the interaction with the external potential, including the electron-nuclei interaction, and the last term is the electron-electron interaction which can be written as

$$E_{ee}\left[\rho(\mathbf{r})\right] = \frac{1}{2}\int \frac{\rho(\mathbf{r})\rho(\mathbf{r}')}{|\mathbf{r}-\mathbf{r}'|}\, d\mathbf{r}d\mathbf{r}' + E_{xc}\left[\rho(\mathbf{r})\right]. \tag{3.16}$$

The first term on the right hand side of (3.16) describes the electron-electron electrostatic interaction, while the second term describes the non-classical exchange-correlation energy.

Kohn and Sham derived a set of single-particle Schrödinger eqnarray by introducing auxiliary wavefunctions ψ_i, with

$$\rho(\mathbf{r}) = \sum_{i=1}^{n} \psi_i^*(\mathbf{r})\psi_i(\mathbf{r}) \tag{3.17}$$

where "n" represents the number of electrons. The kinetic energy is then given by

$$T\left[\rho(\mathbf{r})\right] = -\frac{\hbar^2}{2m}\sum_{i}^{n} \langle\psi_i|\nabla^2|\psi_i\rangle. \tag{3.18}$$

If the wavefunctions are orthonormal, i.e.,

$$\int \psi_i^*(\mathbf{r})\psi_j(\mathbf{r})d\mathbf{r} = \delta_{ij}, \tag{3.19}$$

we can define a functional of the wavefunctions

$$\Omega\left[\psi_i\right] = E\left[\rho(\mathbf{r})\right] - \sum_i \sum_j \epsilon_{ij} \int \psi_i^*(\mathbf{r})\psi_j(\mathbf{r})d\mathbf{r}. \tag{3.20}$$

Here ϵ_{ij} are Lagrange multipliers constraining the wavefunctions to be orthonormal. Minimization of $\Omega[\psi_i]$ with respect to $\psi_i^*(\mathbf{r})$ gives rise to the Kohn-Sham equation,

$$\left[-\frac{\hbar^2}{2m}\nabla^2 + v_{\text{eff}}(\mathbf{r})\right]\psi_i(\mathbf{r}) = \epsilon_i\psi_i(\mathbf{r}) \tag{3.21}$$

with v_{eff} being

$$v_{\text{eff}}(\mathbf{r}) = v(\mathbf{r}) + \int \frac{\rho(\mathbf{r}')}{|\mathbf{r}-\mathbf{r}'|}d\mathbf{r}' + v_{\text{xc}}(\mathbf{r}), \tag{3.22}$$

and $v_{\text{xc}}(\mathbf{r})$ being the exchange-correlation potential given by

$$v_{\text{xc}}(\mathbf{r}) = \frac{\delta E_{\text{xc}}}{\delta\rho(\mathbf{r})}. \tag{3.23}$$

Deriving from (3.20) to (3.21), a unitary transform is applied to make it sure that the wavefunctions $\phi_i(\mathbf{r})$ are orthonormal. A many-body problem is now reduced to solving a single-particle Schrödinger equation (3.21) with an effective local potential v_{eff} defined in (3.22).

3.3.3 Exchange-correlation functional

Although Kohn-Sham theory makes a problem much easier, it is still extremely hard to solve the problem in practice because we do not know explict form of energy functionals. So, it is unavoidable to introduce an approximation to further simplify the problem. For this purpose, we implicitly define the exchange-correlation functional $E_{\text{XC}}[n(\mathbf{r})]$ as below.

$$E_{\text{XC}}[n(\mathbf{r})] = T[n(\mathbf{r})] - T_{\text{s}}[n(\mathbf{r})] + E_{\text{ee}}[n(\mathbf{r})] - E_{\text{H}}[n(\mathbf{r})] \tag{3.24}$$

where $T[n(\mathbf{r})]$ and $E_{\text{ee}}[n(\mathbf{r})]$ are the exact kinetic and electron-electron interaction energies, respectively. The intention for doing this is to make the unknown contribution to the total energy of the non-interacting system as local as possible.

Although E_{XC} makes local contributions, it is turned out that its contribution is still significant being amount to the binding energy of many systems. Therefore, an accurate treatment of exchange and correlation is highly desirable for better predictions of material properties. Recently, there are diverse approximations describing the exchange-correlation potential. Here we will quickly review local density approximation (LDA) and generalized gradient approximation (GGA), which are employed in this thesis.

3.3.4 Local density approximation

LDA is the simplest approximation, yet still having powerful predicting applications in many solids, within which the density can be treated locally as an uniform electron gas. More specifically, it treats the exchange correlation energy at a given point as that of a uniform electron gas having the same density. LDA was originally introduced by Kohn and Sham [20]. It is widely accepted that LDA is a decent approximation soundly working in a slowly varying density. This approximation assumes the exchange-correlation energy for a density $\rho(\mathbf{r})$ to be given by

$$E_{\mathrm{xc}}^{\mathrm{LDA}} = \int \rho(\mathbf{r}) \epsilon_{\mathrm{xc}}^{\mathrm{LDA}}(\rho) d\mathbf{r}. \tag{3.25}$$

Here $\epsilon_{\mathrm{xc}}(\rho)$ is the exchange-correlation energy per particle for an uniform electron gas of density. The exchange-correlation potential is then given by

$$v_{\mathrm{xc}}^{\mathrm{LDA}}[\rho(\mathbf{r})] = \frac{\delta E_{\mathrm{xc}}^{\mathrm{LDA}}}{\delta \rho(\mathbf{r})} = \epsilon_{\mathrm{xc}}^{\mathrm{LDA}}(\rho) + \rho(\mathbf{r}) \frac{\partial \epsilon_{\mathrm{xc}}(\rho)}{\partial \rho}. \tag{3.26}$$

This can then be employed in (3.22) for practical calculations, with the exchange-correlation energy of an uniform electron gas of a given density

$$\epsilon_{\mathrm{xc}}^{\mathrm{LDA}}(\rho) = \epsilon_{\mathrm{x}}^{\mathrm{LDA}}(\rho) + \epsilon_{\mathrm{c}}^{\mathrm{LDA}}(\rho), \tag{3.27}$$

where the exchange potential is given by the Dirac functional [16, 18]

$$\epsilon_x^{\mathrm{LDA}}[\rho(\mathbf{r})] = -\frac{3}{4}\left(\frac{3}{\pi}\right)^{\frac{1}{3}}\rho(\mathbf{r})^{\frac{1}{3}}. \tag{3.28}$$

Accurate estimations for $\epsilon_{\mathrm{c}}(\rho)$ can be obtained from more accurate level of calculations such as **QMC!** (**QMC!**) calculations. These estimations are then interpolated to provide an analytic form for $\epsilon_{\mathrm{c}}(\rho)$. In particular, Perdew and Zunger [22] parameterized the correlation energy based on **QMC!** simulation of Ceperley and Alder [23] as

$$\epsilon_c^{\mathrm{PZ}}(\rho) = \begin{cases} A\ln r_s + B + Cr_s\ln r_s + Dr_s, & r_s < 1, \\ \gamma/(1+\beta_1\sqrt{r_s}+\beta_2 r_s), & r_s > 1, \end{cases} \tag{3.29}$$

where $A = 0.0311$, $B = -0.048$, $C = 0.002$, $D = -0.0116$, $\gamma = -0.1423$, $\beta_1 = 1.0529$, $\beta_2 = 0.334$, and $r_x = (3/4\pi\rho)^{1/3}$ is the average distance between electrons in uniform electron gas.

3.3.5 Generalized-gradient approximations

Success in LDA has lead to the search for better description of the exchange-correlations potential via the modification of LDA. The first step for this modification is to introduce the gradient of the density $|\nabla\rho(\mathbf{r})|$, i.e.,

$$E_{\mathrm{xc}}^{\mathrm{GGA}} = \int \rho(\mathbf{r})\epsilon_{\mathrm{xc}}^{\mathrm{LDA}}(\rho)F_{\mathrm{xc}}(\rho, \nabla\rho, \nabla^2\rho, \cdots)d\mathbf{r}. \tag{3.30}$$

where F_{XC} is an enhancement factor introduced to modify the LDA expression, so that the inhomogeniety in the electron density may be accounted for. Among many other GGAs, Perdew-Burke-Erenzerhof (PBE)-GGA [24] is one of the most popular choices due to its satisfactory conditions for the exchange-correlation hole and single

fitting parameter which is not sensitive to the accuracy of the result. The detailed form of the correlation term within PBE-GGA is given by

$$\epsilon_{\rm c}^{\rm PBE}(\rho) = \int \rho({\rm r}) \left[\epsilon_{\rm c}^{\rm hom}(\rho) + H(\rho, t) \right], \tag{3.31}$$

where $\epsilon_{\rm c}^{\rm hom}(\rho)$ is the correlation energy of homogeneous electron gas, and t is a dimensionless variable of $\rho(\mathbf{r})$ defined by $t = |\nabla\rho|/2\phi k_s \rho$, with $\phi = [(1+\zeta)^{2/3} + (1-\zeta^{2/3}]/2$ and $k_s = \sqrt{4k_F/\pi a_0}$ (the Thomas-Fermi screening wavenumber, $a_0 = \hbar^2/me^2$). The function H is given by

$$H = \frac{e^2}{a_0}\gamma\pi^3 \ln\left[1 + \frac{\beta}{\gamma}t^2\left(\frac{1+At^2}{1+At^2+A^2t^4}\right)\right], \tag{3.32}$$

where

$$A = \frac{\beta}{\gamma}\left[\exp\left(\frac{-\epsilon_{\rm c}^{\rm hom}}{\gamma\pi^3 e^2/a_0}\right) - 1\right]^{-1} \tag{3.33}$$

The detailed form of the exchange term within PBE-GGA is given by

$$E_{\rm x}^{\rm PBE} = \int \rho(\mathbf{r})\epsilon_{\rm xc}^{\rm hom}(\rho) F_{\rm x}(\rho, \nabla\rho, \nabla^2\rho, \cdots) d\mathbf{r}. \tag{3.34}$$

The enhancement factor of $F_{\rm x}$ is given by

$$F_{\rm x} = 1 + \kappa - \frac{\kappa}{(1+\mu s^2/\kappa)}, \tag{3.35}$$

where s is a dimensionless function of $\rho(\mathbf{r})$ defined by $s = |\nabla\rho|/2k_{\rm F}\rho$, and numerical values, κ and μ are 0.804 and 0.21951, respectively.

3.4 Pseudopotential

Electrons in solids can be crudely divided into two kinds, one of which is core electrons and the other is valence electrons. Core electrons are characterized by strong

localization near the closed inner atomic shells, and valence electrons are characterized by living outside the core. Core electrons have a trend to have a large kinetic energy which means large plane waves are required to describe the oscillatory behavior of their wave functions, and it demands a large number of set of plane waves. This means that describing core electrons asks high cost computing power in practice. Therefore, all-electron plane-wave calculations, which describe both core and valence electrons, demand a huge computational expense that is simply not practical. Fortunately, it is found that variations of the electronic structure of the core-electrons in different chemical environments is negligible, thus allowing problems relating to the core-electrons to be overcome by using an alternative ways such as the introduction of pseudopotential approximation [25].

The current pseudopotential approaches can be traced back to the famous paper written by Phillips and Kleinman [26]. They have shown that it is possible to construct a smooth valence wave function $\tilde{\varphi}_v$ which is not orthogonal to the core states φ_c, by combining the core and the true valance wavefunctions φ_v in the following way:

$$|\tilde{\varphi}_v\rangle = |\varphi_v\rangle + \sum_c \alpha_{cv}|\varphi_c\rangle. \tag{3.36}$$

Here $\alpha_{cv} = \langle\varphi_c|\tilde{\varphi}_v\rangle \neq 0$. The wave functions satisfying the modified Schrödinger equation

$$\left[\mathcal{H} + \sum_c (\varepsilon_v - \varepsilon_c)|\varphi_c\rangle\langle\varphi_c|\right]|\tilde{\varphi}_v\rangle = \varepsilon_v|\tilde{\varphi}_v\rangle \tag{3.37}$$

are called pseudo-wave functions, where $\mathcal{H} = \hat{\mathcal{T}} + \hat{\mathcal{V}}$, $\hat{\mathcal{V}} = (Z_c/r)\hat{I}$ is the bare nuclear potential, and $\hat{\mathcal{I}}$ is the identity operator. This indicates that one can construct a

pseudo-Hamiltonian

$$\mathcal{H}_{\mathrm{PS}} = \mathcal{H} + \sum_c (\varepsilon_v - \varepsilon_c)|\varphi_c\rangle\langle\varphi_c| \tag{3.38}$$

with the same eigenvalues of the original Hamiltonian, yet wht much smoother, nodeless wavefunctions near the core of the atoms. The corresponding potential

$$V_{\mathrm{PS}} = \frac{Z_c}{r}\hat{\mathcal{I}} + \sum_c (\varepsilon_v - \varepsilon_c)|\varphi_c\rangle\langle\varphi_c| \tag{3.39}$$

is named as a *pseudopotential*. This pseudopotential acts in different ways on wavefunctions when angular momentum is different. Therefore, the form of a pseudopotential should be angular-momentum dependent, and one of the most general forms is as below.

$$V_{\mathrm{PS}}(\mathbf{r}) = \sum_{l=0}^{\infty}\sum_{m=-l}^{l} v_{\mathrm{PS}}^{l}(r)|lm\rangle\langle lm| = \sum_{l=0}^{\infty} v_{\mathrm{PS}}^{l}(r)P_l. \tag{3.40}$$

where $\langle\mathbf{r}|lm\rangle = Y_{lm}(\theta,\phi)$ are spherical harmonics, $v_{\mathrm{PS}}^{l}(r)$ is the pseudopotential corresponding to the angular component l, and the operator

$$P_l = \sum_{m=-l}^{l} |lm\rangle\langle lm| \tag{3.41}$$

is a projection operator onto the lth angular momentum subspace.

3.4.1 Norm-conserving pseudopotentials

If the all-electron potential and the pseudopotential are the same outside some radius r_c, which is usually called the *cutoff radius*, then the all-electron and pseudo-wavefunctions are proportional if the corresponding logarithmic derivatives are the same

$$\frac{1}{R_{\mathrm{AE}}^{l}}\left[\frac{dR_{\mathrm{AE}}^{l}(\varepsilon,r)}{dr}\right]_{r_c} = \frac{1}{R_{\mathrm{PS}}^{l}}\left[\frac{dR_{\mathrm{PS}}^{l}(\varepsilon,r)}{dr}\right]_{r_c} \tag{3.42}$$

The proportionality becomes an equality only when the pseudo-wavefunctions is further required to preserve the norm inside the cutoff radius

$$\int_0^{r_c} r^2 [R^l_{\rm PS}(\varepsilon, r)]^2 dr = \int_0^{r_c} r^2 [R^l_{\rm AE}(\varepsilon, r)]^2 dr \tag{3.43}$$

This property is called *norm-conservation*, and it was first introduced pseudopotentials by Hamann, Schlüter, and Chaing (HSC) [27].

A key result of HSC was to realize that the norm of the wavefunction also appears in a very important identity related to the Friedel sum rule:

$$-\frac{1}{2}\left\{[rR^l(\varepsilon, r)]^2 \frac{d}{d\varepsilon}\frac{d}{dr}\ln R^l(\varepsilon, r)\right\}_{r_c} = \int_0^{r_c} r^2 [R^l(\varepsilon, r)]^2 dr. \tag{3.44}$$

Therefore, the norm-conservation condition, i.e. the equality of the RHS above for all-electron and pseudo wavefunctions, imposes that, to first-order in the eigenvalue, the logarithmic derivatives of the all-electron and pseudo wavefunctions vary in the same way.

Recently some of the smoothest norm-conserving pseudopotentials are obtained using the recipe by Troullier and Martins [28], who thoroughly studied the convergence properties of the plane wave expansion of the pseudopotential. They generalized Kerker's scheme by proposing the following analytic form of the wavefunction inside the cutoff radius:

$$R^l_{\rm TM}(r) = r^l \exp(p(r)), \tag{3.45}$$

with $p(r) = c_0 + \sum_{i=2}^{n} c_i r^i$. The r^l behavior for small r is included to avoid a hard-core pseudopotential with a singularity at the origin, which would translate into a large number of plane waves, but it is also physically correct.

3.4.2 Kleinman-Bylander separable form

In 1982, Kleinman and Bylander (KB) developed a fully non-local, separable form of the pseudopotential, $\Delta V_{\rm sep}^{l}$ [29], by requesting that its action on the reference pseudo wavefunctions be the same as that of the original, HSC semi-local form $\Delta V_{\rm PS}^{l}$. To this end, they proposed

$$|\zeta_{\rm KB}^{lm}\rangle = |\Delta V_{\rm PS}^{l}. \tag{3.46}$$

By applying the operator $\Delta V_{\rm sep}^{l}$ to the reference pseudo wavefunction $\Delta V_{\rm PS}^{l}$, it is straightforward to prove the requested property, i.e.

$$\Delta V_{\rm KB}^{l}|\Phi_{\rm PS}^{lm}\rangle = \left[\frac{|\Delta V_{\rm PS}^{l}\Phi_{\rm PS}^{lm}\rangle\langle\Phi_{\rm PS}^{lm}\Delta V_{\rm PS}^{l}|}{\langle\Phi_{\rm PS}^{lm}|\Delta V_{\rm PS}^{l}|\Phi_{\rm PS}^{lm}\rangle}\right]|\Phi_{\rm PS}^{lm}\rangle = \Delta V_{\rm PS}^{l}|\Phi_{\rm PS}^{lm}\rangle. \tag{3.47}$$

The Kleinman-Bylander projector is then written as

$$\Delta V_{\rm KB}^{l} = \sum_{m=-l}^{l} E_{\rm KB}^{lm}|\xi_{\rm KB}^{lm}\rangle\langle\xi_{\rm KB}^{lm}|, \tag{3.48}$$

where

$$|\xi_{\rm KB}^{lm}\rangle = \frac{\zeta_{\rm KB}^{lm}}{\langle\zeta_{\rm KB}^{lm}|\zeta_{\rm KB}^{lm}\rangle} \tag{3.49}$$

are normalized projection functions. The strength of the non-locality is determined by the energies $E_{\rm KB}^{lm}$, which are given by

$$E_{\rm KB}^{lm} = \alpha_{lm}\langle\Phi_{\rm PS}^{lm}|(\Delta V_{\rm PS}^{l})^2|\Phi_{\rm PS}^{lm}\rangle \tag{3.50}$$

with

$$\alpha_{lm} = \langle\Phi_{\rm PS}^{lm}|\Delta V_{\rm PS}^{l}|\Phi_{\rm PS}^{lm}\rangle^{-1}. \tag{3.51}$$

3.4.3 Projector augmented waves (PAWs) method

The projector augmented wave method is analogous to pseudopotentials in that it introduces projectors acting on smooth valence functions that are the primary objects in the calculation [30, 31]. It also introduces auxiliary localized functions like the "ultrasoft" pseudopotential method. However, the localized functions actually keep all the information on the core states like the orthogonalized plane wave and augmented plane wave methods. Thus many aspects of the calculations are identical to pseudopotential calculations; e.g. all the operations on smooth functions with fast Fourier transforms, generation of the smooth density, *etc.*, are the same.

The linear transformation to the all-electron valence functions $\psi^v = \mathcal{T}\tilde{\psi}^v$ is assumed to be a sum of non-overlapping atom-centered contributions $\mathcal{T} = \mathcal{I} + \sum_{\mathbf{R}} \mathcal{T}_{\mathbf{R}}$, each localized to a sphere denoted Ω_{vecr}. If the smooth wavefunction is expanded in spherical harmonics inside each sphere,

$$|\tilde{\psi}\rangle = \sum_m c_m |\tilde{\psi}_m\rangle, \tag{3.52}$$

with the corresponding all-electron function,

$$|\psi\rangle = \mathcal{T}|\tilde{\psi}\rangle = \sum_m c_m |\psi_m\rangle. \tag{3.53}$$

Hence the full wavefunction in all space can be written

$$|\psi\rangle = |\tilde{\psi}\rangle + \sum_{\mathbf{R}m} c_{\mathbf{R}m}\{|\psi_{\mathbf{R}m}\rangle - |\tilde{\psi}_{\mathbf{R}m}\rangle\}. \tag{3.54}$$

The energy can be written as a sum of three terms,

$$E_{\text{total}} = \tilde{E}_{\text{total}} + E^1_{\text{total}} + \tilde{E}^1_{\text{total}}, \tag{3.55}$$

where $\tilde{E}$ denotes the energy due to the smooth functions evaluated in Fourier space, $\tilde{E}^1$ denotes the same terms evaluated only in the spheres on radial grids, and E^1 the energy in the spheres with the full functions.

3.5 Basis sets

Both wavefunction and density functional methods aim to compute properties of interest without recourse to experimental data. Doing this requires finding the wavefunction. As this is generally unknown, it is usual to expand it in terms of a set of known functions. A single electron wavefunction can be written as

$$\psi_i(\mathbf{r}) = \sum_{j=1}^{\infty} c_j \phi_j(\mathbf{r}), \tag{3.56}$$

where $\phi_j(\mathbf{r})$ are members of a complete set of functions. Obviously it is impossible to use an infinite number of basis functions so the sum in (3.56) is taken over a finite number of functions. This introduces another source of error into the calculations as it is not then possible to describe components of Ψ along the missing functions.

Any family of functions could, in principle, be used as basis functions. Ideally the basis functions should have the same limiting behavior as the real wavefunction, for an isolated atom or molecules they should decay to zero, and they should be computationally inexpensive.

3.5.1 Plane waves

For solids Bloch's theorem prescribes that the wavefunctions must be composed of a phase factor and a periodic part that verifies $u_{\mathbf{k}}(\mathbf{r}) = u_{\mathbf{k}}(\langle + \mathbf{a}_i)$, with $\mathbf{a}_i$ any lattice vector. This can be used to introduce naturally the basis set of plane waves.

Plane waves are solutions of the Schrödinger equation in the presence of a constant external potential, as is approximately verified in interstitial regions in solids.

In general, any function in real space can be written as the Fourier transform of a function in reciprocal space,

$$u_{\mathbf{k}}(\mathbf{r}) = \int e^{i\mathbf{g}\cdot\mathbf{r}} \tilde{u}_{\mathbf{k}}(\mathbf{g}) d\mathbf{g}, \tag{3.57}$$

but due to the periodicity of $u_{\mathbf{k}}(\mathbf{r})$, the only allowed values of $\mathbf{g}$ are those that verify $e^{i\mathbf{g}\cdot\mathbf{a}_j} = 1$, i.e. $\mathbf{g}\cdot\mathbf{a}_j = 2n\pi$ for $j = 1, 2, 3$ - three lattice vectors. This implies that $\mathbf{g} = n_1\mathbf{b}_1 + n_2\mathbf{b}_2 + n_3\mathbf{b}_3$, where

$$\mathbf{b}_i = 2\pi \frac{\mathbf{a}_j \times \mathbf{a}_k}{\Omega} \tag{3.58}$$

and $\mathbf{n} = (n_1, n_2, n_3)$ is a vector of integer numbers. Therefore, the $\mathbf{g}$ vectors in the Fourier transform (3.57) are restricted precisely to the reciprocal lattice vectors $\mathbf{G}$, and the general expression for the wavefunction is:

$$\varphi^{(\mathbf{k})}(\mathbf{r}) = \frac{e^{i\mathbf{k}\cdot\mathbf{r}}}{\sqrt{\Omega}} \sum_{\mathbf{G}=0}^{\infty} C_{\mathbf{k}}(\mathbf{G}) e^{i\mathbf{G}\cdot\mathbf{r}}. \tag{3.59}$$

Hence, due to the periodicity, the Fourier transform (3.57) becomes a Fourier series, where the Fourier coefficients are $C_{\mathbf{k}}(\mathbf{G})$. This restriction of the possible values of $\mathbf{g}$ to the reciprocal lattice vectors ensures that periodic boundary conditions are automatically verified. We now define the plane wave basis functions

$$\phi_{\mathbf{G}}(\mathbf{r}) = \frac{1}{\sqrt{\Omega}} e^{i\mathbf{k}\cdot\mathbf{r}}, \tag{3.60}$$

which are suitably normalized in the supercell

$$\langle \phi_{\mathbf{G}} | \phi'_{\mathbf{G}} \rangle = \frac{1}{\Omega} \int_{\Omega} e^{i(\mathbf{G}-\mathbf{G}')\cdot\mathbf{r}} d\mathbf{r} = \frac{1}{\Omega}(\Omega \delta_{\mathbf{G},\mathbf{G}'}) = \delta_{\mathbf{G},\mathbf{G}'} \tag{3.61}$$

so that plane waves corresponding to different wave vectors, $\mathbf{G} \neq \mathbf{G}'$, are orthogonal. With this definition, the wavefunctions for the different eigenstates j can be written as

$$\varphi^{(\mathbf{k})}(\mathbf{r}) = e^{i\mathbf{k}\cdot\mathbf{r}} \sum_{\mathbf{G}=0}^{\infty} C_{j\mathbf{k}}(\mathbf{G})\varphi_{\mathbf{G}}(\mathbf{r}). \tag{3.62}$$

For the plane wave calculations, we used Vienna *Ab-initio* Simulation Package (VASP) code [32] and Quantum ESPRESSO package [33].

3.5.2 Pseudo-atomic orbital

The use of plane wave basis set has been more general in the solid state physics community. Recently, however, pseudo-atomic orbital (PAO) based method has attracted lots of attention due to its computational efficiency especially combined with the $O(N)$ method algorithm.

Numerical atomic orbitals was designed to represent localized atomic orbitals on numerical grids. These orbitals are obtained from solving radial Schrödinger equation on numerical grids with a confinement boundary condition. This boundary condition enforce a radial cutoff to the real-space extension of numerical orbitals, which guarantees good localization of a basis set. Also numerical optimization scheme on a basis set, which makes small number of basis orbitals from a larger basis set in maintaining the same accuracy, is possible to reduce a computational cost. These properties combined with the pseudopotential scheme lead to high-performance PAO method. For the PAO calculations, we used the SIESTA code [34].

Kohn-Sham orbital ψ_μ is given by the linear combination of atomic orbitals $\phi_{i\alpha}$:

$$\psi_\mu(\mathbf{r}) = \sum_{i\alpha} c_{\mu,i\alpha}\phi_{i\alpha}(\mathbf{r} - \mathbf{r}_i), \tag{3.63}$$

where i is a site index, $\alpha \equiv (plm)$ an collective orbital index, and $\phi_{i\alpha} \equiv Y_{lm} R_{ipl}$. The basis orbitals are eigenstates of the atomic Kohn-Sham equation with a confinement pseudopotential in a semilocal form for each angular momentum quantum number l.

3.6 Molecular Dynamics

3.6.1 Verlet algorithm

For the time evolution of the system, one of the indispensible ingredient in molecualr dynamics (MD) is the integrator of classical Newtonian equation of motions with discrete time sequence. For this purpose most frequently used integrator is verlet algorithm.[**?**]

$$r(t+\delta t) = r(t) + \delta t v(t) + \frac{1}{2}\delta t^2 a(t) + \frac{1}{6}\delta t^3 b(t) + \cdots \tag{3.64}$$

$$r(t-\delta t) = r(t) - \delta t v(t) + \frac{1}{2}\delta t^2 a(t) - \frac{1}{6}\delta t^3 b(t) + \cdots \tag{3.65}$$

Adding these two Tailor series gives

$$r(t+\delta t) = 2r(t) - r(t-\delta t) + \delta t^2 a(t) \tag{3.66}$$

The Verlet algorithm uses the positions and accelerations at time t, and the position from the previous step, $r(t-\delta t)$, to calculate new positions at $t+\delta t$. The velocities do not explicitly appear in the Verlet integration algorithm. The velocities can be calculated in a variety of ways. For example,

$$v(t) = \frac{r(t+\delta t) - r(t-\delta t)}{2\delta t} \tag{3.67}$$

Alternatively, the velocities can be estimated at the half-step, $t + \frac{1}{2}\delta t$

$$v(t + \frac{1}{2}\delta t) = \frac{r(t + \delta t) - r(t)}{\delta t} \tag{3.68}$$

Several variations on the Verlet algorithm have been developed. One of them is leap-frog Verlet which uses the following relations.

$$v(t + \frac{1}{2}\delta t) = v(t - \frac{1}{2}\delta t) + \delta t a(t) \tag{3.69}$$

$$r(t + \delta t) = r(t) + \delta t v(t + \frac{1}{2}\delta t) \tag{3.70}$$

In this algorithm, the velocities $v(t + \frac{1}{2}\delta t)$ are first calculated from the velocities at time $t - \frac{1}{2}\delta t$ and the accelerations at time t. Then the positions at time $t + \delta t$ are deduced from the velocities just calculated and the positions at time t from the Eq. 3.70. Therefore velocities and positions are in out of phase by the $\frac{1}{2}\delta t$. There is a way to calculate velocities at time t by averaging two velocities.

$$v(t) = \frac{1}{2}[v(t + \frac{1}{2}\delta t) + v(t - \frac{1}{2}\delta t)] \tag{3.71}$$

There is velocity Verlet method which gives the positions, velocities and accelerations at the same time.

$$r(t + \delta t) = r(t) + \delta t v(t) + \frac{1}{2}\delta t^2 a(t) \tag{3.72}$$

$$v(t + \delta t) = v(t) + \frac{1}{2}\delta t[a(t) + a(t + \delta t)] \tag{3.73}$$

As can be seen in Eq. 3.73, the velocity verlet method actually implemented as a three-stage procedure because, to calculate the new velocities requires the accelerations at both t and $t + \delta t$. Therefore in the first step the position at $t + \delta t$ are calculated with the Eq. 3.6.1 using the velocities and the accelerations at time t.

3.6.2 Temperature in MD

The temperature effects in MD simulation are incorporated by the ionic velocity. If the total kinetic energy, $\Sigma mv^2/2$, is equated to $3Nk_BT/2$, which we know is the total thermal energy for N atoms at temperature T, the kinetic temperature which measures the temperature of the system can be defined.

$$T_{kinetic} = \frac{\Sigma mv^2}{3Nk_B} \tag{3.74}$$

If the number of atoms in the system is many enough, i.e. in the thermodynamic limit, each atom's velocity follows the boltzmann distribution in every time step. Atomic velocity and position is determined by the integration of force in each time step. In certain case $T_{kinetic}$ deviate far from the intended temperature. To avoid this, velocities of atoms are rescaled to the intended temperature by multiplying the factor

$$\sqrt{\frac{T_0}{T_{ave}}} \tag{3.75}$$

where T_0 is the desired temperature and $T_{kinetic}$ is the average kinetic temperature since the last velocity rescaling. However, this velocity rescaling does not correspond to any ensemble. Usually, Nose-Hoover (NV) thermostat which built on elegant formalism proposed by Nose is one of the most used one in NVT (constant particle number, volume, temperature) MD. One new variable s which act as a thermal reservoir with the mass Q added to the equations of motion. In this microcanonical dynamics on this extended system is shown to give canonical properties. There is Nose-Hoover chain thermostats in which the ergodicity is improved by thermostatting the thermostat variable.

3.7 Lowdin basis

In analyzing the amount of charges in atom, Lowdin charge population uses "Lowdin-orthogonalized" basis $\{\psi_i\}$ instead of non-orthogonal set $\{\varphi_i\}$ [35].

We introduce $m \times m$ matrice $\mathbf{H}$ and $\mathbf{S}$ with the elements H_{ij} and S_{ij}, and column vector $\mathbf{c}$:

$$\mathbf{c} = \begin{pmatrix} c_1 \\ c_2 \\ \vdots \\ c_i \\ \vdots \\ c_m \end{pmatrix}$$

$$(\mathbf{H} - E\mathbf{S})\mathbf{c} = 0 \tag{3.76}$$

,where $S_{ij} = \langle \varphi_i | \varphi_j \rangle$

$$\{\psi_j\} = \sum_{k=1}^{m} S_{kj}^{-1/2} \varphi_k; \quad j = 1, 2, 3, \ldots, m. \tag{3.77}$$

Then, the matrix elements of the Hamiltonian $\widehat{H}$ in the basis $\{\psi_j\}$ are

$$\langle \psi_i | \widehat{H} | \psi_j \rangle = \langle \sum_k S_{ki}^{-1/2} \varphi_k | \widehat{H} | \sum_l S_{ij}^{-1/2} \varphi_l \rangle \tag{3.78}$$

$$= \sum_{k,l} S_{ik}^{-1/2} H_{kl} S_{ij}^{-1/2} \tag{3.79}$$

$$= H'_{ij} \tag{3.80}$$

Since $\{\varphi_i\}$ and $\{\psi_j\}$ spans same subspace, any function can be expanded with $\{\psi_j\}$ basis. Thus $\{\varphi_i\}$ can also be expanded as

$$\{\varphi_k\} = \sum_l S_{lk}^{+1/2}\{\psi_j\} \quad (k = 1, 2, 3, \ldots, m). \tag{3.81}$$

Therefore, one has

$$\sum_k c_k\varphi_k = \sum_k c_k \sum_l S_{lk}^{1/2}\psi_l = \sum_{k,l}(S_{lk}^{1/2}c_k)\psi_l = \sum_l d_l\psi_l \tag{3.82}$$

where vector $\mathbf{d} = \mathbf{S_c}^{1/2}$. Then the matrices and vectors transform in the new basis $\{\psi_j\}$.

$$\mathbf{H} \to \mathbf{H'} = \mathbf{S}^{-1/2}\mathbf{HS} \tag{3.83}$$

$$\mathbf{S} \to \mathbf{1} \tag{3.84}$$

$$\mathbf{c} \to \mathbf{d} \tag{3.85}$$

Substituting these expressions into 3.76, the solution of the linear variational problem in the orthonormalized basis $\{\psi_j\}$ leads to the "standard" eigenvalue equation

$$\mathbf{H'd} = E\mathbf{d} \tag{3.86}$$

Chapter 4

Silicene on metallic substrates

After the first synthesis of silicene was succeeded on 4x4 Ag (111) surface as 3x3 superlattice in 2012, many researches have focused on Ag (111) surface for silicene substrate. Follow-up studies have found that Si atoms can form silicene on the other metal substrate like ZrB_2 (0001) and Ir (111) and ordered 2D structure on Au (110) [1, 36, 13]. However, all that materials are metal, which are not suitable for utilizing silicene in nanoelectronics. Though many researches are focusing on finding insulating substrate for silicene, no substrates are reported up to now. Even though metal substrate is unusable practically, the studies of silicene on metal substrate can give guide line in designing insulating substrate.

4.1 Calculation detail

The first-principles calculation is performed based on density functional theory (DFT) using VASP (Vienna Ab intio Simulation Package). Projector augmented wave (PAW) method is employed with local density approximation (LDA) and gen-

eralized gradient arrpoximation (GGA) exchange-correlation functionals[4-6]. The cut-off energies of plane-wave basis depend on metal atoms that 400, 350 and 400 eV for Ag, Au and ZrB_2. The force criterion for relaxation convergence is set to 0.01 $eV/$Å. We use crystal-orbital overlap projection (COOP) method, which use orthgonalized molecular orbital, to analyze orbitals' characters in band structure [7]. K-points sampling of Brillouin zone is done based on Monkhorst-Pack scheme [37]. We performed slab calculation in order to investigate the structural and electronic properties of silicene on substrate surface. At first, bulk calculation materials corresponding to each substrates is done to determine simulation conditions (lattice constants, cut-off energy, number of k-point sampling, and exchange-correlation functional). Pre-calculated bulk is cleaved for various direction which is perpendicular to substrate surface (e. g. (001), (111) for ZrB_2 and Ag, respectively) and we obtained five layer substrate due to the restriction of computational costs. During the substrate relaxation, two bottom layers are fixed to mimic semi-infinite bulk. Silicene is put on substrate in various relative positions and full relaxed with substrate except two bottom layers as above mentioned. Though silicene is formed on substrate by the deposition of Si atoms atomically, it is beyond this study.

Since binding energy of deposited Si atoms to substrate and energy barrier of Si atoms on substrate surface are important factors for Si atoms to diffuse on substrate in order to form single layer, we also calculate them for each metallic substrate. The binding energy between deposited Si atoms and substrate is replaced with binding energy between silicene and substrate (*i.e.* silicene formation process is removed.) and it is obtained using the relation.

$$E_{binding} = E_{silicene+substrate} - (E_{silicene} + E_{substrate})$$

The energy barrier of Si atoms on substrate is obtained by calculating the binding energy of Si atom for each grid position during fixing xy-direction coordinates of Si atom. The binding energies of each position can give information how much energy does Si atom need to diffuse on substrate.

4.2 Silicene on Ag (111)

Though Si deposition on Ag surface has been investigated for decades (*e.g.* Silicon nanowire on Ag(110) surface [38]), synthesis of silicon sheet, silicene, on Ag (111) surface is succeeded very recently [39, 8]. The scanning tunneing microscope (STM) images in that experiment is well matched with the results of DFT calculation and LEED that 3 × 3 silicene with 4×4 Ag (111). Besides that superlattice structures, many kinds of silicene superlattice structures on Ag (111) surface have been reported that $\sqrt{11} \times \sqrt{11}$, $2\sqrt{3} \times 2\sqrt{3}$, $\sqrt{7} \times \sqrt{7}$, which depend on the deposition conditions (pressure, temperature and deposition rates) [40, 41]. Among many superlattice structure, we calculate silicene on 4×4 Ag (111) structure, because it is most intensively investigated one in experiments and theories. We also include silicene – Au (111) system because of the similarity in electronic and structural properties between Ag and Au atoms and the results will be given next section briefly.

Figure 4.1 (a)is the optimized structure of 3×3 silicene on 4×4 Ag (111) surface (Four bottom Ag layers are removed and the topmost Ag atoms are shown in the figure for clarity). The heights of 18 Si atoms highly depend on the underneath Ag surface atoms. The Si atoms of silicene can be divided into three groups according to heights and bond orders of Si atoms, and each group contains six Si atoms. Top Si atoms (TS) located directly on surface Ag atoms shift up respect to the other

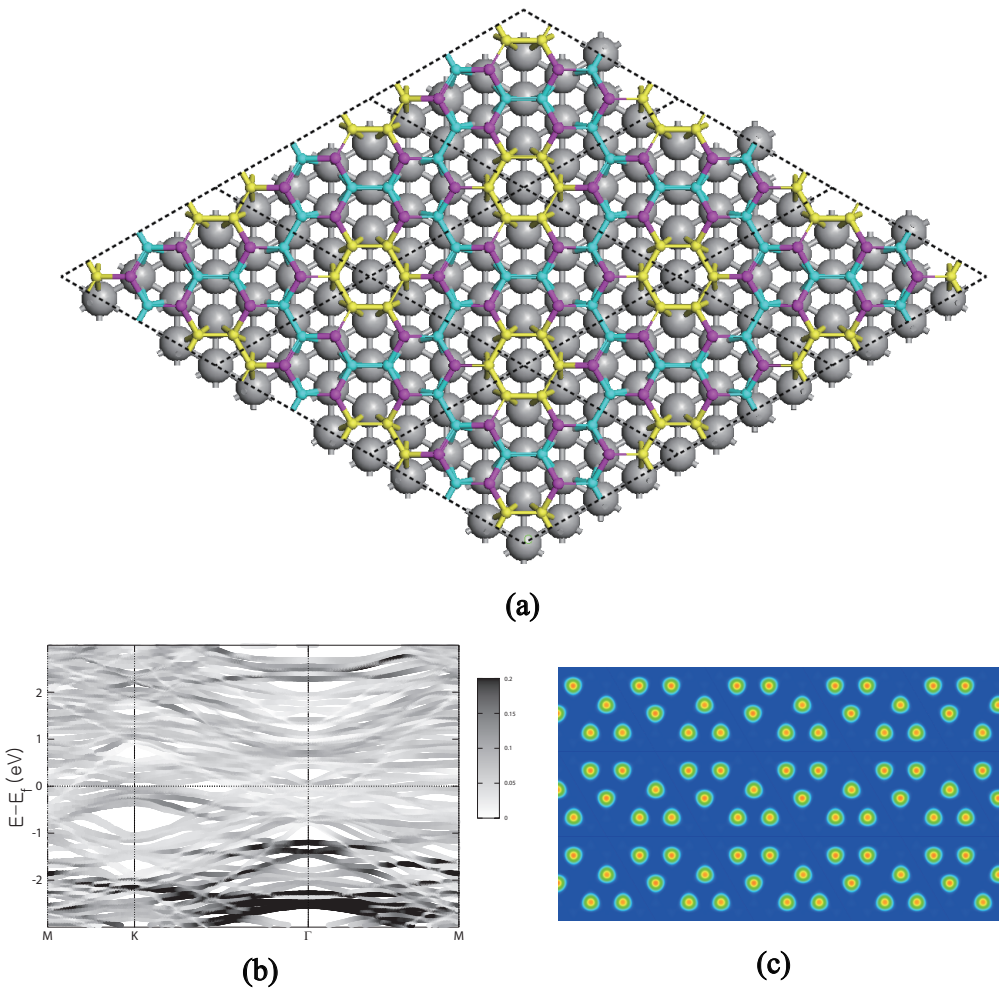

Figure 4.1: Structure of 3×3 silicene on 4×4 Ag (111) surface. (a) 18 Si atoms in silicene are categorized into top Si (TS), middle Si (MS) and bottom Si (BS) according to heights and lateral positions relative to surface Ag atoms. Each TS, MS and BS is represented with cyan, yellow and magenta. (b) Projection of bloch wavefunction to orbital basis shows the contributions of Si $3p_z$ orbital in electronic band structure. The π band from Si $3p_z$ orbital shifts down –1.2eV from Fermi energy due to the charge transfer from Ag substrate to silicene and the bands become flat due to the interaction with Ag substrate. (c) Cross-section of charge density plot, of which energy range is between -1.3 eV and Fermi level around Γ point, at 0.6Åabove the TS. The charge density shows localized p_z orbital of TS and it correspond to top valence band of Si $3p_z$ orbital in (b).

	Charges	Height(Å)
Top Si (TS)	4.05	2.97
Middle Si (MS)	4.22	2.23
Bottom Si (BS)	4.17	2.17

Table 4.1: The result of Lowdin charge analysis for Si atoms of silicene. The amounts of charge transfer from metallic substrate (Ag) depend on heights and relative positions. Since Si atoms receive electron from Ag atoms, π band of silicene shifts down.

atoms. Six bottom Si atoms (BS) bind with on Ag atom together and two middle Si atoms (MS) share only one Ag atoms. Since BS bind with 1.15 Ag atoms per single Si atom, the amount of charge transfer from Ag atoms to BS and MS is similar. The average charges in three group is given in table 4.2 that electrons transfer from Ag substrate to Si atoms and transferred electrons are 0.05e, 0.22e, and 0.17e per Si atom in TS, MS, and BS. It can be predicted that Dirac-cone, which locates at Fermi level for FPS, will shifts down from Fermi level due to the electron transfer. Figure 4.1 (b) is the projection of wavefunction based on planewave basis to Si $3p_z$ orbital basis that shows the contribution of p_z orbital to electronic band structure. The π band is seen below the Fermi level with -1.2 eV that is consistent with previous prediction. Top of π band is flattened, which means that the p_z orbital is localized. Figure 4.1 (c)is charge density plot obtained for energy range within -1.3 eV and Fermi level at around Γ point. The charge densities coincide with p_z orbital of TS.

The binding energies between silicene and Ag (111) substrate are -0.49 (GGA) and -0.72 (LDA) meV per Si atom, respectively. The energy barrier, difference between maximum minimum binding energy, is 0.85 eV.

4.3 Silicene on Au (111)

Since Au is in same group with Ag that has same number of valence electron and the difference of lattice constants between them is less than 1%, we also calculate silicene on Au (111) surface. Furthermore, recent experiment reports the formation of ordered 2D structure with Si atoms on Au (110) surface [36]. Though Au and Ag has similar surface structure, the buckling pattern of silicene on them is different due to the difference of bonding strength. Figure 4.2 (a) shows the structure of silicene on Au (111) surface that only four Si atoms locate on top positions (Four bottom Au layers are removed and the topmost Au atoms are shown in the figure with dark gray for clarity). We can see from fig. 4.2 that the π band of silicene also shifts down 0.5 eV from Fermi level – Ag (111) system, but the band shift is less than that in fig 4.1 (b). This discrepancy can be explained with the electronegativity that the amount of electron transfer from Au atoms in substrate to silicene is small, because electronegativity of Au (2.53) is much higher than that of Si (1.90) and Ag (1.93). Figure 4.2 also shows that the it is more strongly hybridized with Au atoms. The binding energy of silicene with Au (111) surface is about 0.8 eV per Si atom and is higher than with Ag (111) surface slightly. However, the energy barrier difference them is quite large that 0.17 eV on Au surface and 0.85 eV on Ag surface.

4.4 Silicene on ZrB_2

In addition to Ag (111), ZrB_2 (001), which has layered structure consists of Zr and B layer, is another substrate Si atoms can form silicene on it [1]. During the deposition of Si atoms, ZrB_2 surface is reconstructed to 2×2 lattice and $\sqrt{3} \times \sqrt{3}$

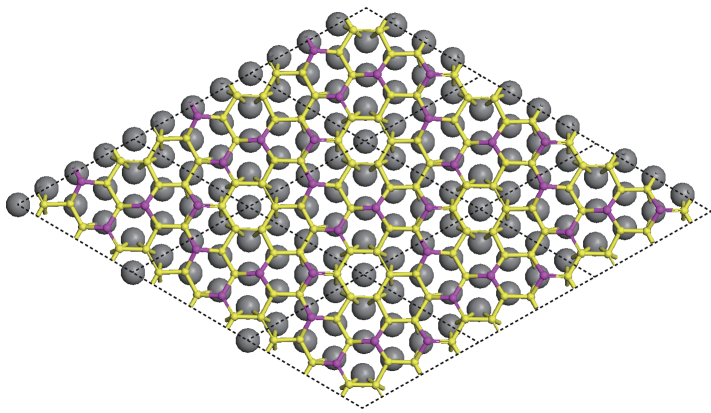

(a)

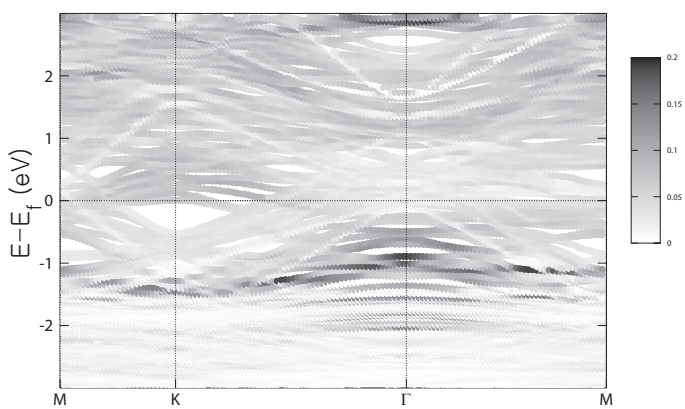

(b)

Figure 4.2: (a) Optimized structure of 3×3 silicene on 4×4 Au (111) surface that consist of four group. Top Si (TS), bottom Si (BS), and surface Au atoms are represent with magenta, yellow, and dark gray, respectively. Due to the difference of bonding strength, the buckling pattern is also different from that of silicene on Ag (111) surface. (b) Projection of bloch wavefunction to orbital basis shows the contributions of Si $3p_z$ orbital in electronic band structure. The Dirac-cone from π band shifts down 0.5 eV from Fermi level like the silicene on Ag (111).

silicene is formed. Small mismatch of lattice constant ($\sim 5\%$) between them makes the height difference of Si atoms in silicene large. The value from DFT calculation is 0.9Åthough the height difference of Si atoms on Ag (111) surface is 0.7Å. Figure 4.3 show the surface structure and binding energies of Si atom to each grid points. The weakest point is coincide with the position of Zr atoms and the binding energy is highest when Si atom locates among Zr atoms, because Si atom can bind with maximum three Zr atoms at that point. The energy barrier, difference between maximum and minimum binding energies, is 0.71 eV.

4.5 Summary

We investigated for the systems of silicene on metallic substrates (Ag, Au and ZrB_2), especially for silicene on Ag substrate. As discussed on **??**, silicene on substrate has deformed buckling patterns and hence the bandgap opens due to the sublattice inversion symmetry breaking. All the electronic band structures of FDS extracted from each systems show bandgap in fig. **??**. 3×3 stilicene on $\sqrt{3} \times \sqrt{3}$ Ag system is chosen among many superlattie structure for silicene on Ag (111) surface. The buckling pattern of silicene changes by interaction with Ag substrate and the Si atoms can be categorized into three groups (TS, MS and BS) depending on heights and planar positions. The bright point in STM image of experiment[8], which applying bias -1.3 eV, coincide with the plot in fig. 4.1 (c). Since the plot is the cross-section of charge density 0.6Åabove the TS and is obtained by summing charge density from -1.3eV to Fermi level at around Γ point, the bright points correspond to p_z orbitals of TS. The projection of plane-wavefunction to Si p_z orbital also shows that π band shifts down to 1.2eV from Fermi level because of electron transfer from Ag substrate

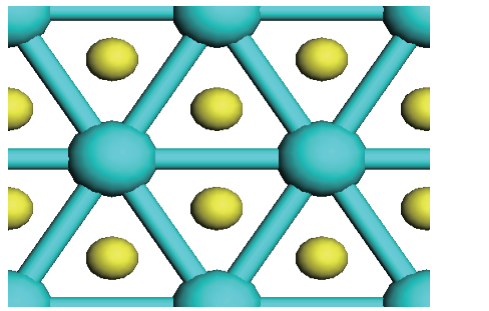

(a)

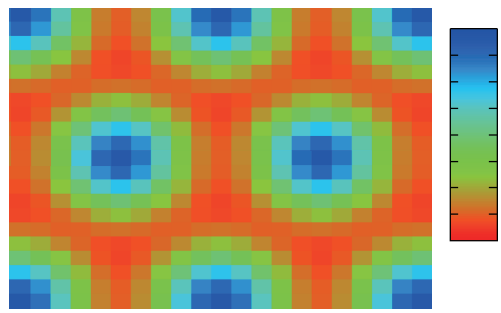

(b)

Figure 4.3: (a) Surface structure of ZrB_2 that Zr (cyan) atoms constitute topmost layer and the B (yellow) atoms next layer. (b) Plot of binding energies for each position and the scale bar represents the strength of binding energy. Binding energy of Si atom directly located on Zr atom shows lowest value. Binding energy difference between maximum and minimum, which act as energy barrier of Si atom on surface, is 0.71 eV

to silicene. Planar position of Silicene on Au (111) substrate is very similar with one on Ag (111) substrate, but the buckling pattern is different due to the difference of bonding strength and hence electronic band structures are also different. Figure 4.4 give electronic band structure of FDS for three substrate ((a) Ag, (b) Au, and (c) ZrB_2).

Comparing the energy barriers in table 4.5 shows that Ag and ZrB_2 on which Si atoms can form silicare have similar values for energy barrier though Au has

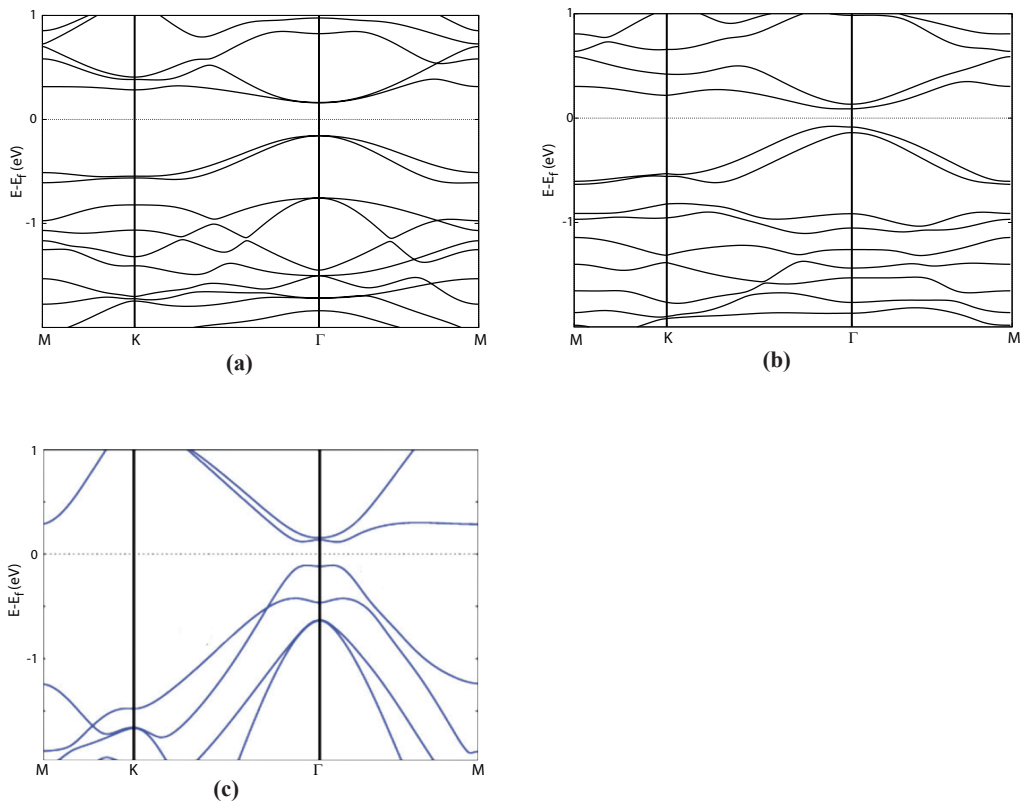

Figure 4.4: Electronic band structures of FDS obtained from (a) Ag, (b) Au, and (c) ZrB_2. ZrB_2 plot is adapted from Ref. [1]. In case of FDS from Au substrate, the deformation breaks all the four-fold degeneracy at Γ point

relatively small value. We can conclude restrictively that substrate for silicene should have energy barrier with ∼0.8 eV.

Substrate	Ag	Au	ZrB_2
Binding energy (eV / Si atom)	0.7	0.8	1.5
Energy barrier (eV)	0.85	0.17	0.70

Table 4.2: The binding energies between silicene and substrate and energy barriers of Si atom on substrate. Ag and ZrB_2 on which Si atoms can form silicare hava similar values for energy barrier though Au has relatively small value.

Chapter 5

silicene on $\sqrt{3} \times \sqrt{3}$ Si (111) - Ag (Au) monolayer

5.1 Introduction

Silicene has attracted much attention as high-performance nanoelectronics, but it has critical problem that silicene has been synthesized only on metallic substrate. Hence, finding insulating substrate for silicene is most important requisite for applying silicene as nanoelectronics. Aside from the above problem, the other problem is revealed that recent studies report that the linear dispersion band from ARPES measurement in experiment [8] is not originated from silicene but from hybridization between silicene and Ag substrate. Measurement of Landau levels using scanning tunneling spectroscopy (STS) does not detect signal of nth Landau level at $E_n \sim \sqrt{n}$, which can be evidence for existence of Dirac fermion. Analysis of elecronic band structure also revelas that π band of FPS and FDS lies between -1.0

eV to 1.0 eV, but the linear band from experiment extends to -3.0 eV. Since Si $3p_z$ orbital is highly mixed with Ag substrate, its character is delocalized all over the space that can not be distinguishable in electronic band structure [42]. The theoretical study shows that the linear band appears only when silicene is present on Ag substrate. The linear band structure also disappears when silicene is removed and hence the result is well agreed with experimental one that it appears after the deposition of silicene on Ag substrate [**?**]. Hence, Ag is not appropriate substrate for silicene in two aspects that it is a metal and hybridizes with silicene too strongly. Considering the above mentioned problems, we can set the requirements for silicene substrate: (1)binds Si atoms strongly enough to prevent Si atoms from aggregation (2)hybridizes with silicene weakly not to destroy Dirac-like band structure around Fermi energy (3)change silicene buckling pattern to break sublattice inversion symmetry and hence open bandgap. We propose metal thin film on insulator as substrate for silicene. The role of thin film is to help deposited Si atoms to form silicene on substrate, but metallic property of film will be suppressed by interacting with insulator. The interaction in substrate can weaken hybridization between silicene and metal atoms in order to prevent the destroy of Dirac-like electron of silicene. Among some candidate materials, we investigate $\sqrt{3} \times \sqrt{3}$ Si (111) – Ag monolayer in this study. We also include $\sqrt{3} \times \sqrt{3}$ Si (111) – Au monolayer due to its similarities in electronic properties with Ag.

5.2 Calculatinal details

The first-principles calculation is performed based on density functional theory (DFT) using VASP (Vienna Ab intio Simulation Package) [32]. Projector augmented

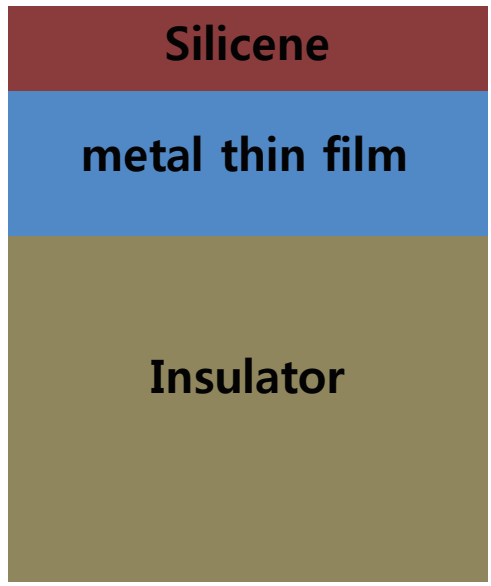

Figure 5.1: Schematic side view. The structure consists of silicene, metal thin film and insulator. Metal thin film helps deposited Si atoms to form silicene, but the metallic property is suppressed due to the interaction with bottom insulator as the carbon buffer layer on SiC acts insulator [2, 3]. The interaction between metal thin film and insulator also may weaken the hybridization between silicene and metal atom.

wave (PAW) method is employed with local density functional (LDA). The cut-off energy of plane-wave basis is 400eV and force criterion for relaxation convergence is 0.01eV/Å. Lowdin charge analysis method, which use orthogonalized molecular basis, is employed to calculate the amount of electron in each atom [43]. We use crystal-orbital overlap projection (COOP) method [44] to analyze orbitals' characters in band structure . 6.62 ×6.62×40 Åsupercell guarantees more than 13Åz-directional vacuum for all calculations. K-points sampling of Brillouin zone is based on Monkhorst-Pack scheme [37]. We use (5×5×1) k-points during geometry optimization and (21×21×1) k-points for density of states (DOS). Since all the sub-

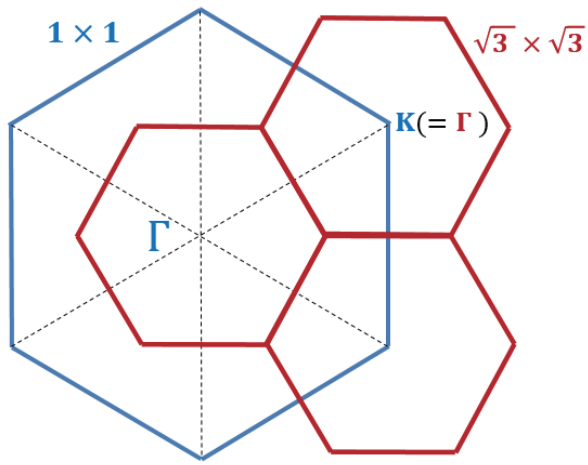

Figure 5.2:

strate and silicene have $\sqrt{3} \times \sqrt{3}$ superlattice structure, special symmetry points of Brillouin zone are folded into reduced brillouin zone (*e.g.* K-point in the primitive cell is folded into Γ point in $\sqrt{3} \times \sqrt{3}$ supercell) The relation is can be seen in fig. 5.2.

5.3 Substrate

We search a substrate consist of insulating material covered with Ag (Au) thin film, because it can satisfy all aforementioned requirements. Topmost Ag layer can possibly guarantee the formation of silicene, but metallic property of Ag layer is suppressed due to the interaction with below insulating material. Furthermore, hybridization between silicene and Ag layer also can be weaken, because Ag layer interacts with insulator too. In this study, we investigate Si (111)-Ag monolayer among a

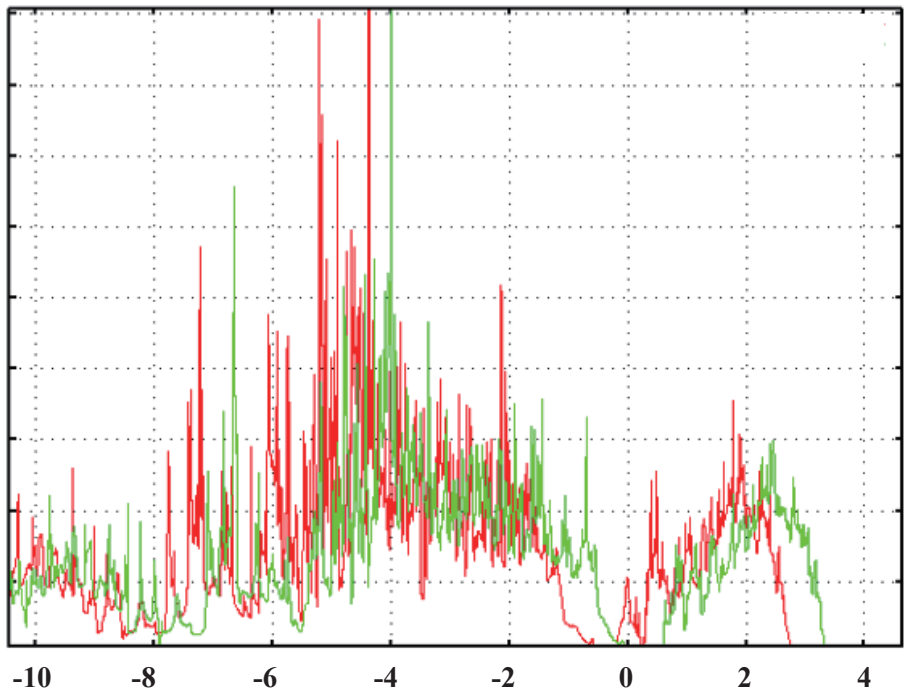

Figure 5.3: Green and red line correspond to Ag one monolayer and 4/3 monolayer, respectively. The density of state (DOS) shift down as one Ag atom is add and the substrate becomes metal.

couple of candidates motivated from the formation of Ag single layer experimentally [45, 46]. A $\sqrt{3} \times \sqrt{3}$ Si (111) slab with seven layers is obtained by cleaving the bulk Si perpendicular to (111)-direction and the bottom layer of slab is terminated with H atoms.The lattice constant of $\sqrt{3} \times \sqrt{3}$ Si(111) slab determined from *abintio* calculation is 6.62Åis very similar with experimental lattice constant, 6.61Å. The total substrate, $\sqrt{3} \times \sqrt{3}$ Si(111) – Ag monolayer (SS), is completed by putting three Ag atoms , which correspond to exact one monolayer, on Si (111) slab per unit cell. If one Ag atom is added in unit cell, which correspond to 1.3 monolayer, additional Ag atom give charge doping effect and the substrate changes to metal as shown in

fig. [**?**]. Two bottom layers of substrate are fixed during relaxation to mimic bulk structure and six top layers of substrate, including Ag monolayer, are full relaxed from various initial configurations. Figure 5.4 (a) shows most stable configuration, inequivalent triangle (IET), which is well agreed with experimental results . Both triangles are nearly equilateral triangles, of which average side lengths are 2.8Åand 3.9Å. Ag atom directly located on the Si atom shift 0.5Åup with respected to the other two Ag atoms. We also calculate for $\sqrt{3} \times \sqrt{3}$ Si(111)–Au monolayer (SG) by replacing Ag atoms with Au atoms and obtain almost same configuration (configuration of Au monolayer is not shown here). Figure 5.4 (b) and (c) show that both substrate (Ag and Au) have indirect bandgaps about 550 meV and 130 meV, respectively.The prominent difference between two band structures is in first conduction bands and hence they are mainly originated from surface states.

5.4 properties of silicene on substrates

5.4.1 Structural and electronic properties

Subsequently, we constitute a total system by putting √3x√3 silicene on the precalculated substrates. Since lattice mismatch between freestanding pristine silicene (6.66Å) and substrate (6.62Å) is less than 1%, contraction of silicene on substrate is negligible. Silicene, Ag (Au) monolayer, and five top layer of Si (111) are full relaxed and two bottom layers in substrate are fixed. Figure 5.5 (a) shows optimized configuration that Si atoms of silicene move during relaxation precess and locate directly on the top Si atoms of Si (111). It can be seen that planar position of silicene strongly depends on the top Si atoms' positions. Intermediated metal atoms

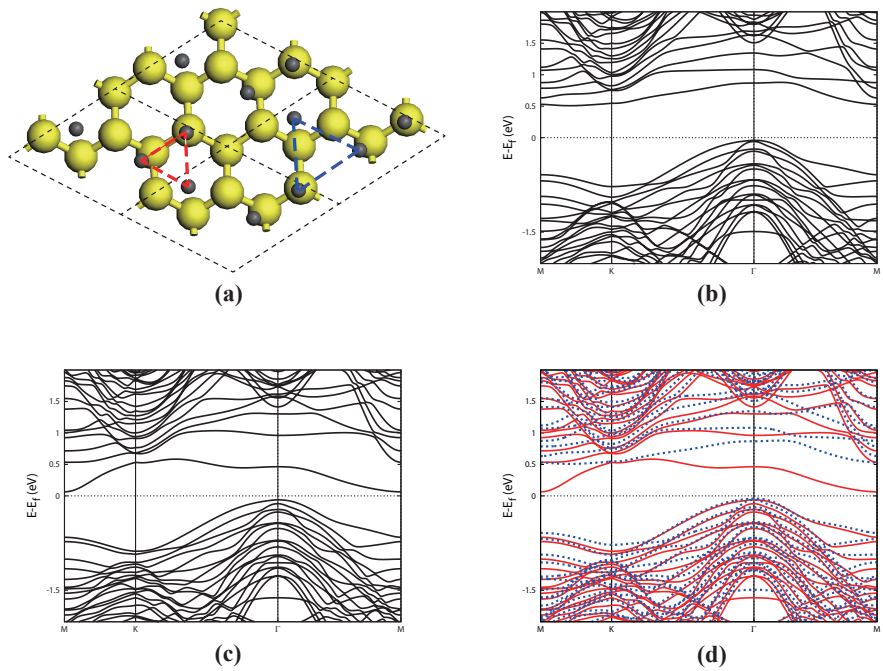

Figure 5.4: (a) top view of IET structure (only topmost Si layer is shown) that Ag and Si atoms are represented with dark gray and yellow. Average side lengths of each inequivalent triangle are 0.28nm (red dotted line) and 0.39nm (blue dotted line). The Ag atom directly located on Si atom shift up with respect to the other two atoms and height difference between them is about 0.5Å. (b), (c) Electronic band structures of substrate for Ag and Au monolayer on Si (111) substrate. The indirect bandgaps are 550 and 130 meV, respectively. (d) Comparison of two band structure, (b) & (c). The differences between them is prominent in first conduction bands, which means that first conduction band is mainly originated from surface states and is modified by interaction with Si (111).

affect the heights of Si atoms of silicene and height difference of top and bottom Si atoms is 1.3Å. Silicene on both substrate (SS, SG) show similar electronic band structure in fig. 5.5 (b) with bandgap $\sim$ 120 meV (Bandgap can be larger, because it is well-known that DFT calculation with LDA functional underestimates bandgap in most cases). We can realized off-current state in silicene nanoelectronics with this bandgap. Since the heights of Si atoms depend on inhomogeneous Ag (Au) monolayer, buckling pattern of silicene on substrate also changes from that of FPS that two Si atoms among six Si atoms in silicene located on Ag atoms shift up respect to the other atoms. Buckling patterns of deformed silicene on substrate and pristine silicene (top and bottom Si atoms are represent with magenta and cyan) are given in fig. 5.6 (a) and (b). Comparing two structure shows that only one Si atom in unit cell shift down, but the band structures are quite different as in fig. 5.6 that changing buckling pattern not only open bangap, 36 meV, but also break degeneracy of Dirac-cone at Γ point.

5.4.2 Band projection on orbital basis

We use COOP method in analyzing orbital character of each atom in first conduction band. For convenience, all atoms are categorized into four groups: silicene $3pi_z$ (SP), Ag monolayer (AM), five top layers of Si slab (ST), two bottom layers of Si slab (SB). We only include $3pi_z$ orbital from silicene, because the other orbitals' characters do not contribute to conducting channel due to strong covalent bonds. Figure 5.7 gives four projection plots that each represents the contributions of corresponding orbitals of atoms. Since we need on-current state that electrons move through π band originated from Silicene p_z orbital, SP dominant energy region ($\sim$ 0.2 eV), E_{on}, is

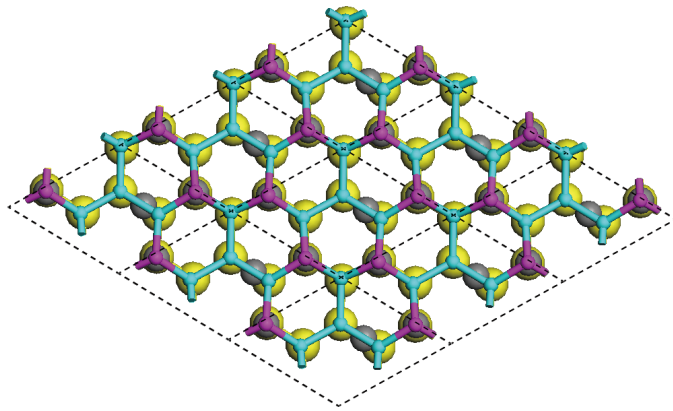

(a)

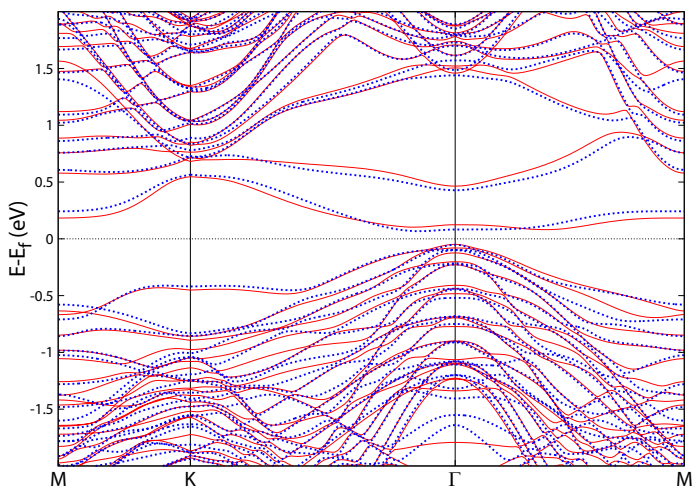

(b)

Figure 5.5: (a)Top view of IET substrate + Silicene. The topmost Si (substrate), Ag (Au), bottom Si (silicene), and top Si (silicene) atoms are represented with yellow, dark gray, cyan, and magenta. Planar and vertical positions of Si atoms in silicene depend on planar positions of uppermost Si atoms of Si (111) substrate and Ag (Au) atoms, respectively. Since Si atoms directly located on Ag (Au) atoms shift up, the buckling pattern of silicene change from that of freestanding pristine silicene (FPS). (b) Comparison of band structures of silicene on Ag (red line) and Au (blue dotted line) monolayer. Since metal atoms (Ag, Au) are intermediated between silicene and Si (111) substrate, the structural and electronic properties of silicene on them is almost same.

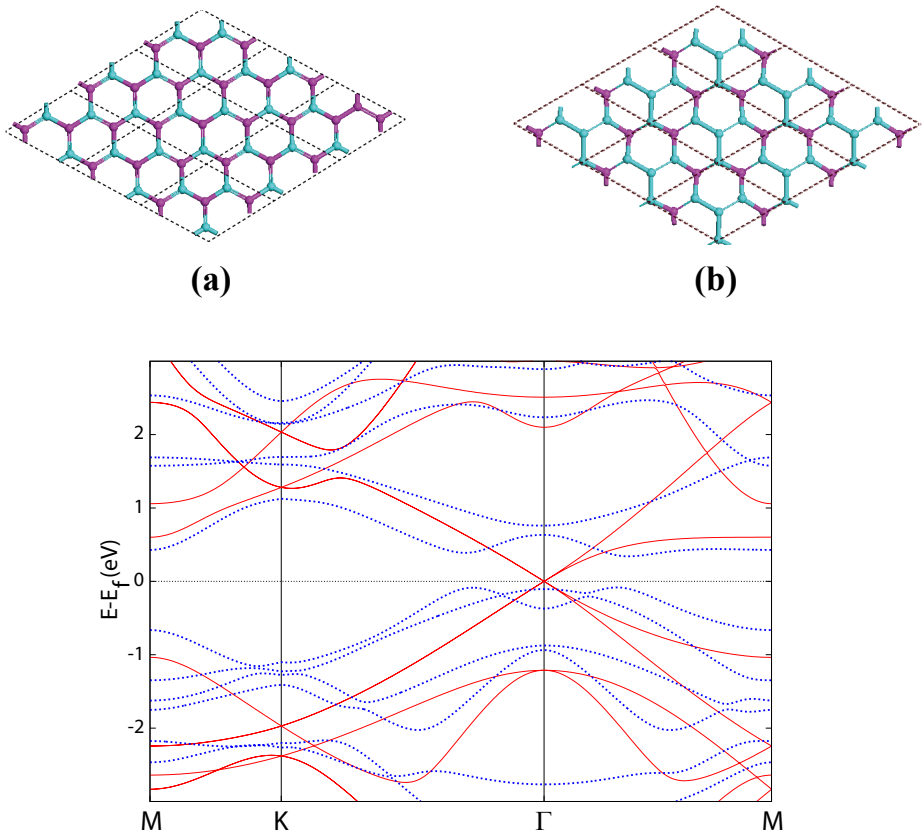

Figure 5.6: Buckling pattern of (a) pristine silicene and (b) deformed silicene by interaction with substrate. Top and bottom Si atoms are represented with magenta and cyan. (c) electronic band structure of pristine (red line) and deform (dotted blue line) silicene when they are in freestanding state. Shift down of one Si atom opens bandgap dand breaks four-fold degeneracy at Γ point

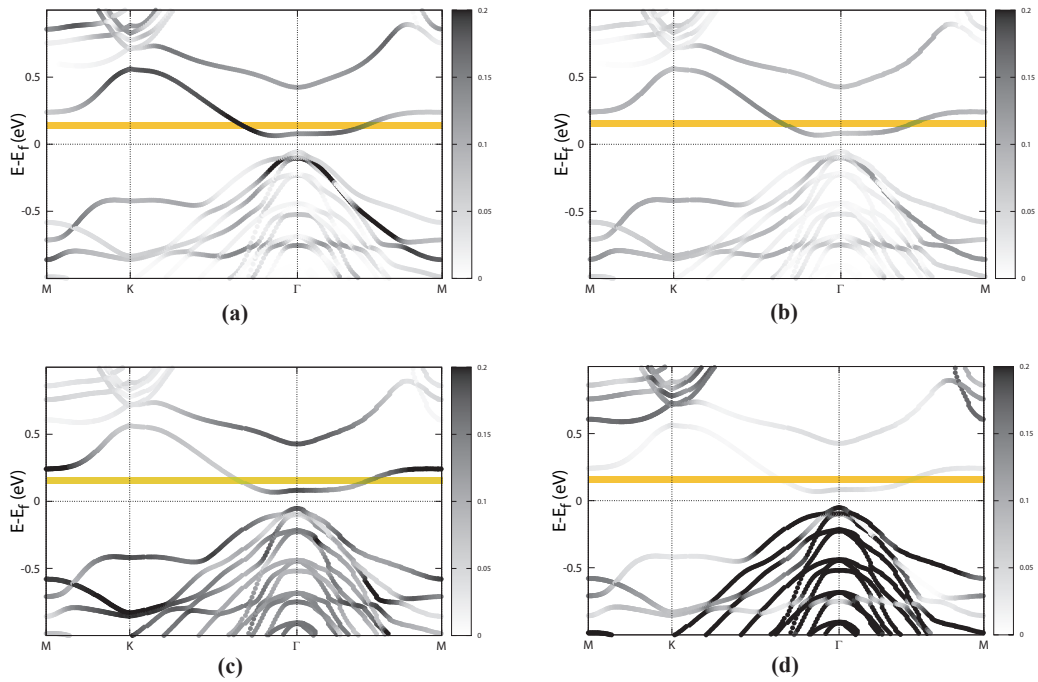

Figure 5.7: Contribution of each group ((a) silicene $3p_z$ (SP), (b) Si (111) five bottom layers (SB), (c) Si (111) two top layers (ST), (d) Ag monolayer (AM)) to band structure. (a) Silicene's contribution is dominant between 0.1 and 0.4 eV, especially around 0.2eV (yellow region). We can use this energy level as on-current state with off-current state at fermi level. (b), (c) Only two Si layers from Si (111) surface can contribute to on-current state and hence the currents can not penetrate to substrate over three layers.

indicated with yellow bar in fig. 5.7. The contribution of SB is negligibly small at E_{on} while AM and ST contribute. This means that current mainly flow through silicene $3p_z$ orbitals, but can not penetrate into substrate more than two layers. (100)-projection of charge density obtained for E_{on} show clearly the contribution of each group in fig. 4.2. Charge density of silicene delocalized along silicene planar direction and hybridized with Ag atom, too. However, Si atoms in substrates have no electron states at E_{on}.The Fermi velocity derived from slope of electronic band

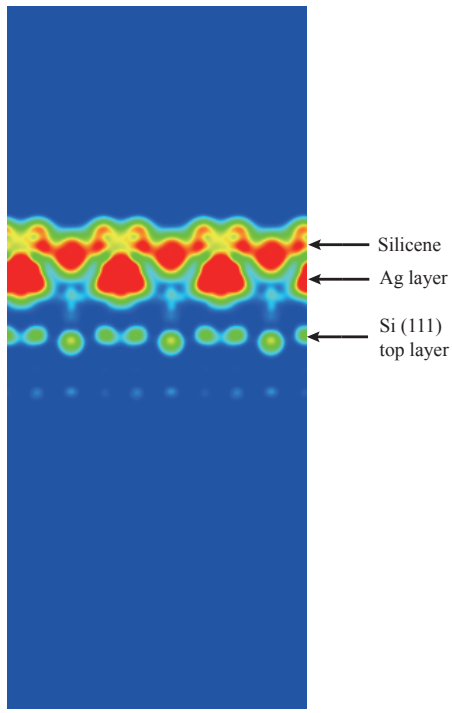

Figure 5.8: Projection to (100) direction of charge density which corresponds to 0.2 eV from Fermi level. Si atoms of silicene has delocalized state along silicene plane and hybridize with highly localized Ag orbitals. Since six bottom layers has no states for that energy level, current can not penetrate substrate deeply.

structure at E_{on} is 0.25 times smaller than that of graphene ar Dirac-cone.

Figure 5.9 show the projected band structure to each group. Though SP character is dominant around ~ 0.15 eV, the energy range is very narrow. Furthermore, strong interaction of silicene to substrate gives more flat band. The Fermi velocity of E_{on} is 0.15 times smaller than that of graphene. Thus, $\sqrt{3} \times \sqrt{3}$ Si (111) - Au monolayer is less favorable than $\sqrt{3} \times \sqrt{3}$ Si (111) - Au monolayer as insulating substrate for silicene. We also compare the binding energies between silicene and each substrate in order to check whether si(111)-Ag and Au monolayer and (4×4)

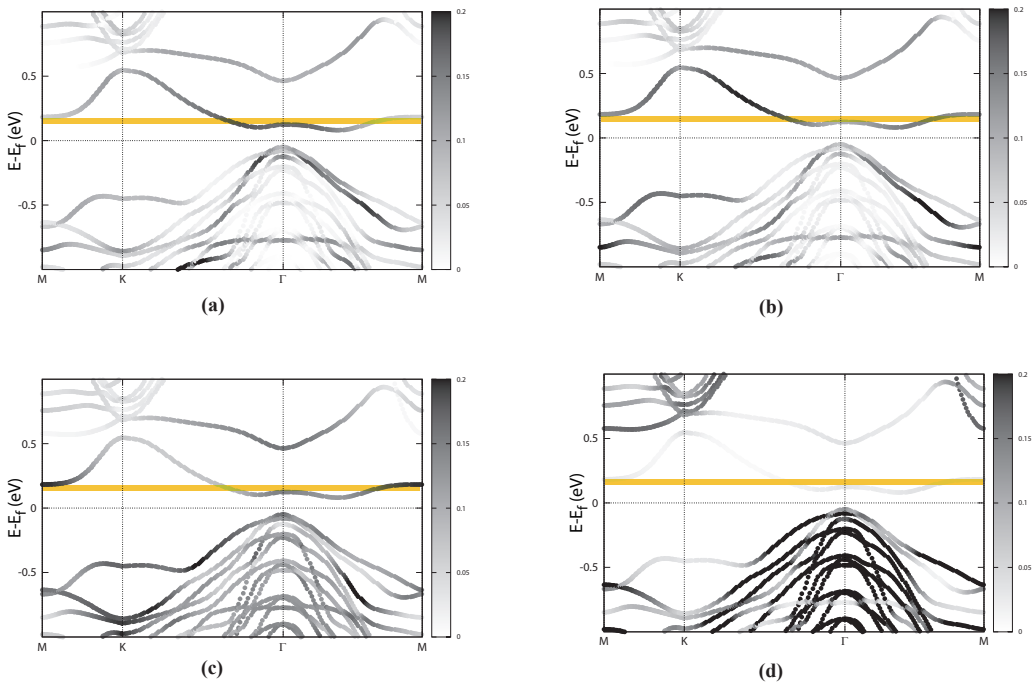

Figure 5.9: Contribution of each group ((a) silicene $3p_z$, (b) Si (111) five bottom layers, (c) Si (111) two top layers, (d) Ag monolayer) to band structure. (a) Silicene's contribution is dominant between 0.1 and 0.4 eV, especially around 0.2eV (yellow region). We can use this energy level as on-current state with off-current state at fermi level. (b), (c) Only two Si layers from Si (111) surface can contribute to on-current state and hence the currents can not penetrate to substrate over three layers.

Ag (111). The binding energies of silicene to substrates are 680meV (851meV) per one Si atom, which are not much deviated from binding energy, 720meV, between silicene and 4×4 Ag (111) substrate. Though kinetics and energy barrier of surface also should be considered to verify if deposited Si atoms form silicene on substrate, we restrict the discussion with binding energy, because surface configuration of metal atoms changes severely when additional Si atom approachs, we can not obtained reasonable energy barrier with same method in 4 However, it can be possibly expect that the energy barriers between SS and Ag(111) surface are not different

considerably, because both surfaces consist of same Ag atoms.

5.5 Summary and conclusions

We have investigated the possibility of $\sqrt{3} \times \sqrt{3}$ Si (111) – Ag (Au) monolayer as an insulating substrate for silicene. Ag atoms on Si (111) surface form IET structure consistent with experimental results and Au atoms form same structure. Both substrates are composed of two parts: bottom Si (111) makes substrate to be insulator and top metal(Ag and Au) monolayers help deposited Si atoms can form monolayer, silicene. Since the binding energies between silicene and substrates are not much different from silicene – 4×4 Ag (111) system and , they are expected to be able to and enable silicene for applying as FET. Ag and Au atoms on Si (111) surface form IET structure which is consistent with experiments. Band structures of both Ag and Au substrates show bandgap with 550 and 130 meV, respectively. The prominent difference between them is shown in first conduction band due to the hybridization between Ag (Au) monolayer and Si (111). When we put freestanding silicene on pre-calculated substrates with various configurations respect to substrate, Si atoms in silicene displace during relaxation to locate on the same planar position with topmost surface Si atoms of Si (111). The heights of them are dependent on Ag atoms that Si atom directly on Ag atom is higher than the other Si atoms with 0.9Å. buckling pattern changes and the system also show bandgap about 120meV for both monolayers. The badgaps are smaller than those of substrate because of the hybridization between silicene and substrate. The COOP analysis reveals that Si $3p_z$ character of silicene is dominant among the another atoms between Γ and K points in first conduction band whereas Si orbital characters in substrate is domi-

nant around K. Thus we can obtain off- and on-current state with $\sqrt{3} \times \sqrt{3}$ Si (111) – Ag monolayer.

Chapter 6

Summary and conclusion

In summary, we have investigated the metallic substrate (Ag (111), Au (111), and ZrB_2 (001)) and the possibility of $\sqrt{3} \times \sqrt{3}$ Si (111) – Ag (Au) monolayer as an insulating substrate for silicene. Lowdin charge anaysis show that electron transfer from Ag (111) to silicene make the π band shift down to 1.2eV from Fermi level and hence the linear dispersion band measured in experiment [8] is not orginated from silicene alone, but from hybridization of silicene and Ag atoms. The energy barrier of Ag (111) and ZrB_2 (001) surface have similar values about $\sim$ 0.8eV. Since energy barrier affect to diffusion of deposited atom, it should be identified in theoretical research.

When silicene is put on substrates, $\sqrt{3} \times \sqrt{3}$ Si (111) – Ag (Au) monolayer, both system shows similar bandgap ($\sim$ 120 meV). We can use this bandgap region as off-current state in utilizing silicene - substrate as nanoelectronics. We analyze the first conduction band to find energy region for on-curent state. The COOP analysis reveals that the contribution of Si $3p_z$ orbital of silicene is most dominant at 0.3 eV

in first conduction band. Since the other atoms have no electron states or localized states, electron can move through delocalized Si $3p_z$ orbital, π band. Hence, on-current state also can be obtained in this system. We show that silicene on $\sqrt{3} \times \sqrt{3}$ Si (111) – Ag monolayer can realized off- and on-current states and hence can act as nanoelectronics.

Oxidation and diffusion of Si atoms, which are important problems practically, will be discussed in the other study

Bibliography

[1] Antoine Fleurence, Rainer Friedlein, Taisuke Ozaki, Hiroyuki Kawai, Ying Wang, and Yukiko Yamada-Takamura. Experimental evidence for epitaxial silicene on diboride thin films. *Phys. Rev. Lett.*, 108:245501, Jun 2012.

[2] H. Yang, A. J. Mayne, C. Cejas, G. Dujardin, and Y. Kuk. Manipulation at a distance: Atomic-scale observation of ballistic electron transport in single layer graphene. *Applied Physics Letters*, 102(22):223104, 2013.

[3] Seungchul Kim, Jisoon Ihm, Hyoung Joon Choi, and Young-Woo Son. Origin of anomalous electronic structures of epitaxial graphene on silicon carbide. *Phys. Rev. Lett.*, 100:176802, Apr 2008.

[4] Andrea F. Young and Philip Kim. Quantum interference and klein tunneling in graphene heterojunctions. *Nature physics*, 5:222, 2009.

[5] Horst L. Stormer Yuanbo Zhang, Yan-Wen Tan and Philip Kim. Experimental observation of the quantum hall effect and berry's phase in graphene. *Nature*, 438:201, 2005.

[6] Kyozaburo Takeda and Kenji Shiraishi. Theoretical possibility of stage corru-

gation in si and ge analogs of graphite. *Phys. Rev. B*, 50:14916–14922, Nov 1994.

[7] S. Cahangirov, M. Topsakal, E. Aktürk, H. Şahin, and S. Ciraci. Two- and one-dimensional honeycomb structures of silicon and germanium. *Phys. Rev. Lett.*, 102:236804, Jun 2009.

[8] Patrick Vogt, Paola De Padova, Claudio Quaresima, Jose Avila, Emmanouil Frantzeskakis, Maria Carmen Asensio, Andrea Resta, Bénédicte Ealet, and Guy Le Lay. Silicene: Compelling experimental evidence for graphenelike two-dimensional silicon. *Phys. Rev. Lett.*, 108:155501, Apr 2012.

[9] Boubekeur Lalmi, Hamid Oughaddou, Hanna Enriquez, Abdelkader Kara, Sebastien Vizzini, Benidicte Ealet, and Bernard Aufray. Epitaxial growth of a silicene sheet. *Applied Physics Letters*, 97(22):223109, 2010.

[10] Baojie Feng, Zijing Ding, Sheng Meng, Yugui Yao, Xiaoyue He, Peng Cheng, Lan Chen, and Kehui Wu. Evidence of silicene in honeycomb structures of silicon on ag(111). *Nano Letters*, 12(7):3507–3511, 2012.

[11] Antoine Fleurence, Rainer Friedlein, Taisuke Ozaki, Hiroyuki Kawai, Ying Wang, and Yukiko Yamada-Takamura. Experimental evidence for epitaxial silicene on diboride thin films. *Phys. Rev. Lett.*, 108:245501, Jun 2012.

[12] Lan Chen, Cheng-Cheng Liu, Baojie Feng, Xiaoyue He, Peng Cheng, Zijing Ding, Sheng Meng, Yugui Yao, and Kehui Wu. Evidence for dirac fermions in a honeycomb lattice based on silicon. *Phys. Rev. Lett.*, 109:056804, Aug 2012.

[13] Lei Meng, Yeliang Wang, Lizhi Zhang, Shixuan Du, Rongting Wu, Linfei Li, Yi Zhang, Geng Li, Haitao Zhou, Werner A. Hofer, and Hong-Jun Gao. Buckled silicene formation on ir(111). *Nano Letters*, 13(2):685–690, 2013.

[14] Eugene Kogan. Symmetry classification of energy bands in graphene and silicene. *Graphene*, 2:74, 2013.

[15] N. D. Drummond, V. Zólyomi, and V. I. Fal'ko. Electrically tunable band gap in silicene. *Phys. Rev. B*, 85:075423, Feb 2012.

[16] Richard M. Martin. *Electronic Structure: Basic Theory and Practical Methods*. Cambridge University Press, Cambridge, 2004.

[17] J. Kohanoff. *Electronic Structure Calculations for Solids and Molecules*. Cambridge University Press, Cambridge, 2006.

[18] R. G. Parr and G. Yang. *Density Functional Theory of Atoms and Molecules*. Oxford University Press, Oxford, 1989.

[19] P. Hohenberg and W. Kohn. Inhomogeneous Electron Gas. *Phys. Rev.*, 136:B864–B871, Nov 1964.

[20] W. Kohn and L. J. Sham. Self-Consistent Equations Including Exchange and Correlation Effects. *Phys. Rev.*, 140:A1133–A1138, Nov 1965.

[21] R. O. Jones and O. Gunnarsson. The density functional formalism, its applications and prospects. *Rev. Mod. Phys.*, 61:689–746, Jul 1989.

[22] J. P. Perdew and A. Zunger. *Phys. Rev. B*, 23:5048, 1981.

[23] D. M. Ceperley and B. J. Alder. Ground State of the Electron Gas by a Stochastic Method. *Phys. Rev. Lett.*, 45:566–569, Aug 1980.

[24] John P. Perdew, Kieron Burke, and Matthias Ernzerhof. Generalized gradient approximation made simple [phys. rev. lett. 77, 3865 (1996)]. *Phys. Rev. Lett.*, 78:1396–1396, Feb 1997.

[25] James C. Phillips. Energy-Band Interpolation Scheme Based on a Pseudopotential. *Phys. Rev.*, 112:685–695, Nov 1958.

[26] James C. Phillips and Leonard Kleinman. New Method for Calculating Wave Functions in Crystals and Molecules. *Phys. Rev.*, 116:287–294, Oct 1959.

[27] D. R. Hamann, M. Schlüter, and C. Chiang. Norm-Conserving Pseudopotentials. *Phys. Rev. Lett.*, 43:1494–1497, Nov 1979.

[28] N. Troullier and José Luriaas Martins. Efficient pseudopotentials for plane-wave calculations. *Phys. Rev. B*, 43:1993–2006, Jan 1991.

[29] Leonard Kleinman and D. M. Bylander. Efficacious Form for Model Pseudopotentials. *Phys. Rev. Lett.*, 48:1425–1428, May 1982.

[30] P. E. Blöchl. Projector augmented-wave method. *Phys. Rev. B*, 50:17953–17979, Dec 1994.

[31] G. Kresse and D. Joubert. From ultrasoft pseudopotentials to the projector augmented-wave method. *Phys. Rev. B*, 59:1758–1775, Jan 1999.

[32] Georg Kresse, Martijn Marsman, and Jürgen Furthmüller. VASP group. *http://cms.mpi.univie.ac.at/vasp*, 2011.

[33] Paolo Giannozzi, Stefano Baroni, Nicola Bonini, Matteo Calandra, Roberto Car, Carlo Cavazzoni, Davide Ceresoli, Guido L Chiarotti, and Matteo Cococcioni. QUANTUM ESPRESSO: a modular and open-source software project for quantum simulations of materials. *Journal of Physics: Condensed Matter*, 21(39):395502 (19pp), 2009.

[34] Josó M Soler, Emilio Artacho, Julian D Gale, Alberto García, Javier Junquera, Pablo Ordejón, and Daniel Sánchez-Portal. The siesta method for ab initio order- n materials simulation. *Journal of Physics: Condensed Matter*, 14(11):2745, 2002.

[35] *SIMPLE THEOREM, PROOFS, AND DERIVATTIONS IN QUANTUM CHEMISTRY*. •, 1943.

[36] Yi Ding and Yanli Wang. Electronic structures of silicene/gas heterosheets. *Applied Physics Letters*, 103(4):043114, 2013.

[37] Hendrik J. Monkhorst and James D. Pack. Special points for brillouin-zone integrations. *Phys. Rev. B*, 13:5188–5192, Jun 1976.

[38] C. Leandri, G. Le Lay, B. Aufray, C. Girardeaux, J. Avila, M.E. Dávila, M.C. Asensio, C. Ottaviani, and A. Cricenti. Self-aligned silicon quantum wires on ag(110). *Surface Science*, 574(1):L9 – L15, 2005.

[39] Abdelkader Kara, Hanna Enriquez, Ari P. Seitsonen, L.C. Lew Yan Voon, Sébastien Vizzini, Bernard Aufray, and Hamid Oughaddou. A review on silicene — new candidate for electronics. *Surface Science Reports*, 67(1):1 – 18, 2012.

[40] H Jamgotchian, Y Colignon, N Hamzaoui, B Ealet, J Y Hoarau, B Aufray, and J P Bibérian. Growth of silicene layers on ag(111): unexpected effect of the substrate temperature. *Journal of Physics: Condensed Matter*, 24(17):172001, 2012.

[41] Chun-Liang Lin, Ryuichi Arafune, Kazuaki Kawahara, Noriyuki Tsukahara, Emi Minamitani, Yousoo Kim, Noriaki Takagi, and Maki Kawai. Structure of silicene grown on ag(111). *Applied Physics Express*, 5(4):045802, 2012.

[42] Chun-Liang Lin, Ryuichi Arafune, Kazuaki Kawahara, Mao Kanno, Noriyuki Tsukahara, Emi Minamitani, Yousoo Kim, Maki Kawai, and Noriaki Takagi. Substrate-induced symmetry breaking in silicene. *Phys. Rev. Lett.*, 110:076801, Feb 2013.

[43] Per-Olov Lowdin. On the non-orthogonality problem connected with the use fo atomic wave functions in the theory of molecules and crystals. *J. Chem. Phys*, 18:365, 1950.

[44] Timothy Hughbanks and Roald Hoffmann. Chains of trans-edge-sharing molybdenum octahedra: metal-metal bonding in extended systems. *Journal of the American Chemical Society*, 105(11):3528–3537, 1983.

[45] Shuji Hasegawa, Norio Sato, Ichiro Shiraki, Cristian L. Petersen, Peter Bøggild, Torben M. Hansen, Tadaaki Nagao, and François Grey. Surface-state bands on silicon si(111)-$\sqrt{3} \times \sqrt{3}$-ag surface superstructure. *Japanese Journal of Applied Physics*, 39(Part 1, No. 6B):3815–3822, 2000.

[46] R. I. G. Uhrberg, H. M. Zhang, T. Balasubramanian, E. Landemark, and H. W. Yeom. Photoelectron spectroscopy study of Ag/Si(111)$\sqrt{3} \times \sqrt{3}$ and the effect of additional ag adatoms. *Phys. Rev. B*, 65:081305, Feb 2002.

국문초록

이차원 벌집 격자구조를 가지는 그래핀은 실험적으로 발견된 이후로 그 독특한 구조적, 전자적 성질때문에 많은 관심을 받고 있다. 탄소와 같은 갯수의 원자가 전자를 갖는 실리콘에 대해서 이론적 연구를 통하여 이차원 벌집 격자 구조에 대한 성질이 예측 (디락 고깔의 존재와 좌굴된 구조)되었으며 최근에는 실리신을 은 (111) 표면 위에서 합성하였다. 이후에 많은 연구가 진행되어 은 (111) 표면 위에서 다양한 초격자 구조를 발견하였으며 다른 금속 표면 위에서도 실리신 합성이 성공하였다. 이러한 실험적 성공으로 인해 실리신은 유망한 나노소자로 기대받고 있지만 여전히 절연체 기판 위에서는 실리신 합성이 보고되지 않고 있다. 또한 기존에 실험에서 각분해광전자분광을 통해 확인한 선형 밴드 구조도 실리신 $3p_z$ 오비탈이 아닌 실리신-은 궤도함수 혼성에 의한 것이라고 보고되고 있다.

이 연구에서는 제일원리 계산을 통하여 독립적으로 놓인 실리신, 실리신-금속 기판 구조에 대한 분석과 함께 실리신 - 절연기판 구조를 제시한다.첫째로, 독립적으로 놓인 실리신은 그래핀과 달리 주기적으로 좌굴된 구조를 가지므로 다양한 방법을 통해 밴드갭을 열릴 수 있음을 보인다: (1) 좌굴 양식이 바뀌는 경우 구조적으로 부격자의 반전대칭이 깨지므로 밴드갭이 열리게 된다. (2) 실리신 평면에 수직한 방향으로 전기장을 걸어주는 경우에도 위, 아래에 위치한 실리콘 원자는 각각 다른 에너지 하에 놓이게 되므로 각 원자들의 파동함수는 달라지므로 마찬가지로

밴드갭이 열린다. (3) 실리신과 기판과사이의 궤도 혼성을 통해서도 밴드갭은 열릴 수 있다. 실제로는 세 가지 모두 밴드갭을 여는데 관여하게 된다.

다음으로 실리신이 은 (111) 표면 위에서 형성된 경우 각 원자들의 전하량을 분석하면 은 기판으로부터 평균 0.15개의 전자가 실리콘 원자로 이동한다. 따라서 실리콘에 원자에 의한 밴드는 전자 밴드 구조에서 아래로 낼려감을 예측할 수 있다. 실제로 전자밴드 구조를 실리콘의 p_z궤도에 시키면 -1.2eV 내려 감을 확인할 수 있다. 따라서 앞 실험에서 -0.3에서 -3 eV까지 걸쳐져 있던 선형분산밴드는 실리신에 의한 것이 아니라는 것을 알 수 있다. 은과 마찬가지로 실리신을 금 (111) 표면에 얹으면 전자의 이동으로 인해 실리콘의 밴드는 아래로 이동하게 되며 전자밴드구조에서 실리신과 금의 궤도 혼성이 더 강하다는 것을 알 수 있다. 표면에 증착된 원자들이 확산하는 데 중요한 요소인 에너지 장벽의 크기를 구해보면 은과 지르코늄 표면은 비슷한 값을 보이지만 금은 훨씬 낮은 값을 보였다. 따라서 일반적으로 사용하는 증착 조건에서 표면의 에너지 장벽의 크기 조건을 대략적으로 제시할 수 있다.

마지막으로 실리신을 $\sqrt{3}\times\sqrt{3}$ 실리콘 (111) 표면 위에 은 또는 금 단일층을 쌓은 기판 위에 얹었을 때의 구조 및 전자적 성질을 연구하였다. 실리신은 상기 기판 위에서 위에서 언급한 세 가지 원인에 의해 120meV 정도의 밴드갭이 열리게 되므로 나노소자에서 꺼짐 상태를 구현할 수 있게 된다. 첫번재 전도대의 특성을 살펴보기 위하여 평면파 기준에서 계산된 궤도함수를 실리콘 원자의 p_z 궤도에 투영시키면 이 궤도가 전자 밴드 구조의 각 부분에 기여하는 정도를 알 수 있다. 실리콘 원자의 p_z 궤도는 K 와 Γ 점 사이, 페르미 준위에서 0.2eV 위에 있는 첫번째 전도대 영역에서 지배적인 영향을 미치게 된다. 따라서 해당하는 에너지 영역을 나노 소자의 켜짐 상태로 구현할 수 있음을 보인다.

주요어 : 범밀도함수이론, 그래핀, 실리신, 나노소자, 절연 기판, 밴드갭, 주사현미경

학번 : 2002-20419